ANNUAL REVIEWS

Annual Review of Chemical and Biomolecular Engineering

Nonconjugated Redox-Active Polymers: Electron Transfer Mechanisms, Energy Storage, and Chemical Versatility

Ting Ma,[1] Alexandra D. Easley,[2] Ratul Mitra Thakur,[1] Khirabdhi T. Mohanty,[1] Chen Wang,[1] and Jodie L. Lutkenhaus[1,2]

[1]Artie McFerrin Department of Chemical Engineering, Texas A&M University, College Station, Texas, USA; email: jodie.lutkenhaus@tamu.edu

[2]Department of Materials Science and Engineering, Texas A&M University, College Station, Texas, USA

Annu. Rev. Chem. Biomol. Eng. 2023. 14:187–216

The *Annual Review of Chemical and Biomolecular Engineering* is online at chembioeng.annualreviews.org

https://doi.org/10.1146/annurev-chembioeng-092220-111121

Keywords

nonconjugated redox-active polymers, batteries, electron transfer kinetics, conductivity

Abstract

The storage of electric energy in a safe and environmentally friendly way is of ever-growing importance for a modern, technology-based society. With future pressures predicted for batteries that contain strategic metals, there is increasing interest in metal-free electrode materials. Among candidate materials, nonconjugated redox-active polymers (NC-RAPs) have advantages in terms of cost-effectiveness, good processability, unique electrochemical properties, and precise tuning for different battery chemistries. Here, we review the current state of the art regarding the mechanisms of redox kinetics, molecular design, synthesis, and application of NC-RAPs in electrochemical energy storage and conversion. Different redox chemistries are compared, including polyquinones, polyimides, polyketones, sulfur-containing polymers, radical-containing polymers, polyphenylamines, polyphenazines, polyphenothiazines, polyphenoxazines, and polyviologens. We close with cell design principles considering electrolyte optimization and cell configuration. Finally, we point to fundamental and applied areas of future promise for designer NC-RAPs.

1. INTRODUCTION

Predicted global shortages and supply chain pressures over strategic elements for lithium-ion batteries (e.g., lithium, cobalt, nickel) have inspired the exploration of organic batteries around the world. With the promise of reducing or eliminating the use of these strategic elements, organic batteries use redox-active small molecules or polymers as active materials in the positive and negative electrodes. More specifically, p-type and n-type redox-active polymers have been proposed in place of transition metal oxides (e.g., $LiNi_xMn_yCo_zO_2$) and graphite. For organic batteries, a broad selection of electrolytes—including traditional nonaqueous lithium-ion battery electrolytes, nonaqueous organic electrolytes that offer a completely metal-free approach, or aqueous-based electrolytes for improved safety or biomedical applications—are available. For organic redox-flow batteries, highly soluble species are desirable, and small, redox-active molecules are advantageous. For organic batteries with solid electrodes, insoluble species are desirable, and high–molar mass, polymeric, redox-active molecules are advantageous.

In this review, we focus on nonconjugated redox-active polymers (NC-RAPs) as active materials in organic batteries with solid electrodes. This broad class can be defined further according to the placement of the redox-active group either in the polymer's backbone or as a pendant group (**Figure 1**). These structural differences impart different chemical and physical properties, redox reactions, and performances. Polymers with the redox-active group in the backbone tend to be more compact (i.e., less free volume), and some can exhibit π-π stacking and larger structural order. A variety of redox-active groups can be incorporated into a nonconjugated backbone, with sulfur being one example gaining significant attention recently. In contrast, polymers with redox-active pendant groups tend to be amorphous with free volume for electrolyte penetration. Representative redox-active pendant polymers include quinone, imide, ketone, sulfur, radical, phenylamine, phenazine, phenothiazine, phenoxazine, and viologen compounds. In separate reviews by us and others (1–6), synthetic methods for redox-active polymers have been discussed.

In general, NC-RAPs have flat, battery-like voltage profiles in discharge due to the localized nature of the electronic charge at the redox site. This behavior is in distinct contrast to conjugated polymers, which distribute charge over the polymer's backbone, leading to a sloping, capacitor-like

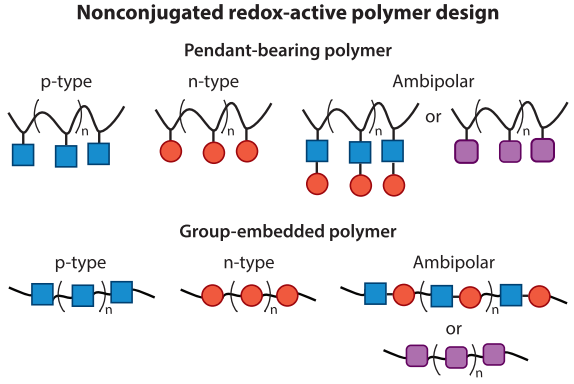

Figure 1

Examples of common nonconjugated redox-active polymer architectures, in which the redox-active group is incorporated as a pendant group or embedded in the polymer backbone. Ambipolar polymers use both p-type and n-type redox-active groups in each repeat unit or a single ambipolar redox-active group. Blue squares, red circles, and purple squares denote a p-type, n-type, and ambipolar redox-active groups.

voltage profile in discharge. On the other hand, the delocalized charge of conjugated polymers results in electronic conductivity that is beneficial in a battery environment. By extension, the localized nature of charge in NC-RAPs can present a barrier to electron transport, which manifests as a relatively low electrical conductivity.

This review first examines the nature of electron transport and transfer in NC-RAPs to better understand how conductivity and kinetics might be improved. Then, the select polymer chemistries are discussed in the context of whether they compensate charge generated by redox reactions using cations (p-type), anions (n-type), or both cations and anions (ambipolar). The review closes with cell design consideration and future prospects.

2. ELECTRON TRANSFER KINETICS AND ELECTRONIC CONDUCTIVITY

Important considerations in the design of NC-RAPS for batteries are the kinetics of electron transfer and conductivity. Fast electron transfer kinetics imply fast charging, which is highly desirable for electric vehicle applications, and high electronic conductivity reduces the need for carbon additives within the electrode and increases the active material loading. In practice, NC-RAPS have fast electron transfer kinetics but low conductivity—two features that might seem contradictory. This is because the redox-active groups have low activation barriers to electron transfer (leading to fast kinetics), but the nonconjugated or insulating mass within the material reduces the net density of charge carriers (leading to low conductivity). Therefore, immense opportunities exist for improving both conductivity and kinetics by molecular design, as discussed below.

2.1. Electron Transfer Kinetics

Consider a pure NC-RAP without any additives cast upon a metallic current collector. During the redox process, generated charge travels within the NC-RAP and then across the NC-RAP–current collector interface. The former process is described by the electron self-exchange rate constant (k_{ex}), and the latter process by the heterogeneous rate constant (k^0). Electron transfer for either homogeneous or heterogeneous processes typically occurs in three main steps: (step 1) diffusion of the redox-active species, (step 2) molecular reorientation (solvent dipoles and resonant electronic structure of the redox-active molecules), and (step 3) electron transfer either to another redox-active group (self-exchange) or to the current collector (heterogeneous) (**Figure 2*a***). In general, the apparent kinetics are classified into instances of kinetic control and fast diffusion, diffusion control from the polymer, and bounded diffusion through pendant groups in which the polymer's backbone is immobile.

To estimate k_{ex} in NC-RAPs, the most commonly used theories/models are Dahms–Ruff theory (7, 8), the diffusion-cooperative model (9), Laviron–Andrieux–Savéant (LAS) theory (10, 11), and Marcus–Hush theory (12–16) (**Figure 2*b***). k_{ex} can be represented as the first and second steps in **Figure 2*a*** occurring in parallel: an activation-limited rate constant (k_{act}) and a diffusion-limited rate constant (k_{diff}), as shown in Equation 1:

$$\frac{1}{k_{ex}} = \frac{1}{k_{act}} + \frac{1}{k_{diff}}. \qquad 1.$$

For a purely activation-controlled reaction, k_{act} is estimated using the theory and equations from Marcus and Hush, which represent the redox-active group as a localized sphere (12, 14–16), as shown in Equation 2:

$$k_{act} = K_a \left[\left(\frac{\pi}{\lambda k_B T} \right)^{1/2} \left(\frac{H_{AB}^2}{\hbar} \right) \exp\left(-\frac{\Delta G^*}{k_B T} \right) \right], \qquad 2.$$

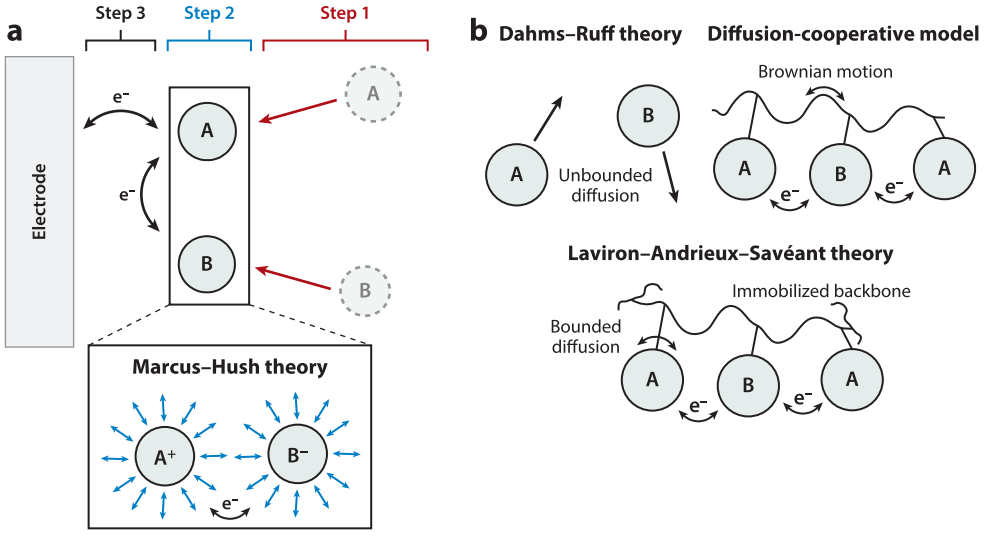

Figure 2

(*a*) Simplified schematic of electron transfer. (*b*) Representation of diffusion scenarios described by three primary theories of electron transfer.

where K_a is the association constant, λ is the reorganization energy, k_B is the Boltzmann constant, T is temperature, H_{AB} is the electronic coupling, $\hbar$ is the reduced Planck constant, and ΔG^* is the activation energy for the transition state. For electron transfer between the same redox-active groups, ΔG^* can be approximated by $(\lambda - 2H_{AB})^2/4\lambda$ (17).

In contrast, for a purely diffusion-controlled reaction, k_{diff} depends on physical diffusion present within the polymer system. For example, using the Smoluchowski model of rigid sphere reactants (18, 19), Dahms and Ruff described k_{diff} as depending on the solution-state physical diffusion of the redox-active molecule (D_A) following Equation 3:

$$k_{diff} = 8\pi a D_A N_A, \qquad 3.$$

where a is the radius of the redox-active group and N_A is Avogadro's number. In contrast, Sato et al. (9) proposed that k_{diff} depended on the Brownian motion of the polymer backbone following Equation 4:

$$k_{diff} = 16\pi a D_{pbys} N_A. \qquad 4.$$

Finally, when the physical diffusion coefficient (D_{pbys}) of the redox-active moieties is further restricted through immobilization ($D_{pbys} \approx 0$), LAS theory is used to determine k_{ex} (10, 11). This typically has been used to describe electron transfer in crosslinked NC-RAPs or those covalently linked to the current collector surface. Additional comparisons for determining k_{diff} are provided in **Supplemental Table 1**, along with the associated assumptions, representative polymer systems, and original constants proposed for each model.

Supplemental Material >

To estimate k^0, Marcus–Hush theory can be applied (Equation 5). However, NC-RAPs in the solid state exhibit low diffusion, so considering the physical diffusion coefficient of the polymer becomes important (Equation 6):

$$k^0 = \kappa_{el} K_p v_n \exp\left(-\frac{\lambda}{4k_B T}\right) \qquad 5.$$

$$k^0 = \kappa_{el} \frac{3D_{pbys}}{2L} \exp\left(-\frac{\lambda}{4k_B T}\right), \quad 6.$$

where κ_{el} is the electronic transmission coefficient, K_p is the precursor equilibrium constant, ν_n is the effective nuclear frequency, and L is the mean distance between redox-active groups.

When determining the correct model/theory to represent the polymer system being studied, one should consider (*a*) the amount of solvent that is present in the polymer film (solvent uptake/swelling), (*b*) the temperature of testing compared to the polymer's glass transition temperature (T_g), and (*c*) the physical diffusion of the redox-active species. When a polymer film has little-to-no solvent uptake and is tested below T_g, the polymer backbone is considered immobile or slow moving, and bounded diffusion of the redox-active groups in the polymer system occurs. For this scenario, LAS theory or the diffusion-cooperative model may best represent the energy barriers to electron transfer in the system. However, once a polymer is tested above T_g or with large solvent uptake, the redox-active groups have significantly more diffusion, which is comparable to the case of free diffusion presented by the Marcus–Hush and Dahms–Ruff theories. There are also exceptions to these cases, where the above theories must be combined (20) or other factors such as electron tunneling must be considered (21).

2.2. Experimental Determination of Kinetic Rate Parameters

The preceding section provided theories and models to estimate electron transfer rates. Experimentally, these can be accessed through various electrochemical measurements. Most commonly, chronoamperometry (CA), cyclic voltammetry (CV), and electrochemical impedance spectroscopy (EIS) are used together to determine both the k^0 and k_{ex} rate constants and apparent diffusion coefficient (D_{app}) in three-electrode cell configurations.

CA consists of a potential step from below the half-wave potential ($E_{1/2}$) to an overpotential of at least 0.25 V (22) (**Figure 3**). The current is then plotted against $t^{-1/2}$, and a linear fit at short timescales ($t \leq 0.5$ s) is applied (23). Assuming semi-infinite diffusion, the linear fit follows the Cottrell equation (Equation 7) and is used to estimate the D_{app} (9):

$$i = \frac{nFAC_E}{\sqrt{\pi t}} \sqrt{D_{app}}, \quad 7.$$

where i is the current output from CA, n is the number of electrons transferred per repeat unit, A is the electrode area, and C_E is the total concentration of redox sites (mol/cm^3). Similar to the Cottrell approach, chronocoulometry can also be used to obtain D_{app} following the method previously reported by Anson (23). As an alternative to using CA to obtain D_{app}, CV can yield D_{app} using the Randles–Sevcik equation by considering the peak current at multiple scan rates (24, 25).

Supplemental Material >

After estimation of D_{app}, k_{ex} is determined an appropriate model (see **Supplemental Table 1**). For example, following the Dahms–Ruff model, k_{ex} is described as

$$k_{ex} = \frac{6\left(D_{app} - D_{pbys}\right)}{C_E \delta^2}, \quad 8.$$

where δ is the average redox site distance, which can be estimated by $\delta = (C_E N_A)^{-1/3}$ (26). D_{pbys} can be estimated experimentally using dynamic light scattering to obtain the physical diffusion of the NC-RAP in solution or using computational methods (9). Depending on the physical diffusion of the redox-active pendant groups, Equation 8 can be simplified to a few different models (summarized in **Supplemental Table 1**). If the polymer is above its T_g or highly solvated, the redox-active pendant groups will exhibit relatively high diffusion, and the Dahms–Ruff equation or diffusion-cooperative model could be applicable. In contrast, if the polymer is below T_g, minimally solvated, or highly crosslinked/bound to the electrode surface, the LAS model could be used.

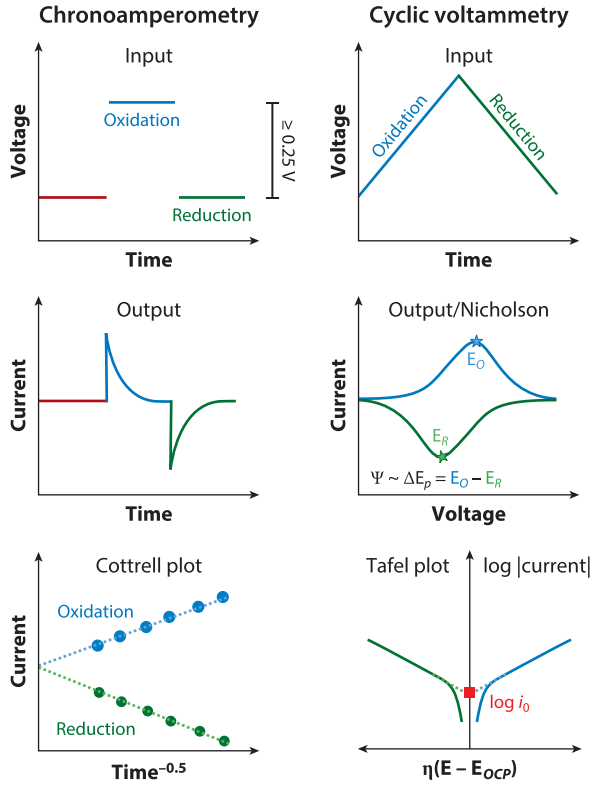

Figure 3

Input and output data/plots for (*left*) chronoamperometry (CA) and (*right*) cyclic voltammetry (CV) experiments. To analyze the output CA data, the Cottrell plot and slope are typically used. CV data can be analyzed using the Nicholson method (peak separation at a single scan rate) or the Butler–Volmer method (by identifying the exchange current from the Tafel plot).

With knowledge of D_{app}, CV can then be performed to determine k^0 using the Nicholson method (27), the Butler–Volmer method (28), the Gileadi method (29), or the method proposed by Klingler & Kochi (30). The Nicholson method (Equation 9) is typically preferred due to the easy determination of ΔE_p (27); however, the Butler–Volmer method (Equation 10) has also been used frequently for corrosion-prevention coatings (**Figure 3**). Following the method of Nicholson, peak separation (ΔE_p) at a known scan rate (v in V/s) is used to determine the value of the rate parameter (ψ) (31):

$$\psi = \frac{k^0}{(\pi D_{app} f v)^{1/2}}, \quad 9.$$

$$i_0 = nFAk^0 C_E. \quad 10.$$

Where i_0 is the exchange current, $f = F/RT$ (F is Faraday's constant and R is the gas constant). Using the Cottrell equation and the method of Nicholson described above, electron transfer kinetics have been studied previously for systems such as nitroxide-based polymers and poly(vinyldibenzothiophenesulfone) (9, 32–34).

Taken together, electrochemical kinetic theory and experiment for NC-RAPs inform us that the reorganization energy should be low, the proximal distance between two neighboring redox

sites should be low, and the polymer's mobility should be high for maximized kinetics. However, theory does not describe the full macroscale behavior completely. For example, the theory presented here applies largely to intramolecular electron transport, but intermolecular phenomena can contribute strongly as well.

2.3. Electrical Conductivity

Generally, the electrical conductivity of NC-RAPs is not as widely described or characterized as its kinetics. There are different ex situ and in situ techniques to measure polymer conductivity, which vary in suitability depending on the polymer's resistance. For example, four-point probe is often used for conjugated polymers, but NC-RAPs are too resistive for this technique. Microelectrodes can circumvent this challenge by reducing the resistance of the tested region. EIS can provide an electrical conductivity, but it is challenging to deconvolute individual ionic and electronic contributions. Both four-point probe and impedance spectroscopy can be useful for solid-state applications. However, in the battery environment, the polymer is in contact with liquid electrolyte and can swell. In that case, it is important to assess conductivity in the swollen state (35–37). We have applied this method successfully to monitor changes in conductance, doping level, and swelling of poly(3-hexylthiophene) in tandem with electrochemical quartz crystal microbalance (38), and such an approach could easily be extended to NC-RAPs.

NC-RAPs typically do not have high electrical conductivity because of their insulating components, which lowers the density of charge carrier sites. The solid-state electrical conductivity of nonconjugated radical polymers such as poly(2,2,6,6-tetramethylpiperidinyloxy-4-yl) (PTMA) is in the range of 10^{-5} to 10^{-11} S/cm (39, 40) but 0.2 S/cm for poly(4-glycidyloxy-2,2,6,6-tetramethylpiperidine-1-oxyl) (PTEO, length scales <600 nm) (41). Yu et al. (42) demonstrated mixed ionic and electron conduction in amorphous, radical-containing polymers by selectively tuning the pendant group chemistry by adding ionic dopant lithium bis(trifluoromethanesulfonyl)imide salt (LiTFSI), yielding a maximum ionic conductivity of 10^{-3} S/cm for the PTEO at elevated temperature. They also observed an increase in electrical conductivity to 0.95×10^{-5} S/cm for PTEO-LiTFSI (10 wt%), which was 10 times higher than for a pristine PTEO film. Ionic conductivity was measured by EIS, whereas electrical conductivity was measured from current-voltage plots (I-V) using Cr/Au electrodes. Joo et al. (43) showed the effect of thermal annealing in an inert environment on the electrical conductivity of PTEO, where PTEO conductivity increased from $\sim 10^{-6}$ S/m to 0.2 S/m. Rostro et al. (39) achieved an electrical conductivity of 1.5×10^{-5} S/cm for PTMA by controlling the chemical nature of the functional pendant group via oxidation, showing that an optimum mixture of nitroxide radicals and oxoammonium cations improved conductivity. Tanaka et al. (44) reported that incorporating radical pendants such as galvinoxyl and phenoxyl onto a polythiophene backbone enhanced the electrical conductivity of the polymer. The electrical conductivity of the precursor polythiophene increased from 2.5×10^{-9} S/cm to 3.6×10^{-6} S/cm as radical content increased to 0.93 radicals/monomer unit because the radical groups facilitated interchain hole transfer. However, Zhang et al. (45) studied polythiophenes with varying content of pendant 2,2,6,6-tetramethylpiperidine-1-oxyl (TEMPO) attached and observed that conductivity decreased exponentially from 7×10^{-5} S/cm to 3.8×10^{-11} S/cm with increasing TEMPO radical content (0–80%). The radical sites caused steric distortions to the conjugated polymer, modifying the intra- and interchain hopping conductivity. Further investigating these polymers, we have shown in an electrochemical cell that redox moieties such as TEMPO attached to a conjugated polymer such as P3HT can undergo internal charge transfer, which results in poor charge storage capacity (46).

Taken together, NC-RAP electrical conductivity remains challenging to improve, but important emerging literature suggests promising approaches. These include lowering the T_g of the

polymer (thereby improving the physical diffusion of the charge carrier sites), reducing the mass of the nonconducting components, increasing the density or proximity of charge carrier sites, or adding charge mediators. In the future, it will be important to consider polymer conductivity in the battery environment, not just the dry, solid state.

3. NC-RAP CHEMISTRIES

NC-RAP chemistries are extremely versatile in that small molecular modifications to the core functional groups can lead to large changes in redox potential and performance. We describe certain redox-active chemistries of interest classified as n-type, p-type, or ambipolar. With the large variety of redox-active cores to choose from, it is impossible to cover them all. Instead, we highlight certain chemistries that have demonstrated promise in recent years in the literature. Regardless of whether their charge compensation occurs with cations, anions, or both, the mechanism of electron transfer in NC-RAPs remains largely the same, as described above.

3.1. N-Type NC-RAPs

During the redox process, cations (positively charged ions) are introduced into the polymer matrix to compensate for the charge imbalance caused by the presence of redox-active groups. The cations serve as counterions and help to stabilize the polymer, allowing for efficient electron transfer between redox-active groups. Here, we summarize certain classes of n-type polymers.

3.1.1. Polyquinones. Polyquinones (PQs) are attractive energy storage materials for their (*a*) high specific capacity derived from the two carbonyl active sites, (*b*) fast kinetics of the tautomerism between carbonyls and enols, (*c*) stable amorphous structure and electrochemical reversibility, and (*d*) diverse and easily tunable molecular structure. Charge is generally compensated by cations from the electrolyte (or protons, in the case of aqueous conditions). Representative PQs and corresponding electrochemical performance are summarized in **Figure 4** and **Supplemental Table 2**.

Supplemental Material >

In early reports, electrochemical polymerization was obtained to yield PQs with a polyaniline-type backbone (PANQ, PDAQ, PADAQ) (47–49). Because the redox reaction of polyaniline occurred at a higher potential, the conductive backbone improved the rate performance without affecting the redox chemistry of the quinone system. However, these PQ electrodes exhibited poor cycling stability due to the dissolution of the redox-active polymers.

Later, poly(anthraquinonylsulfide) (PAQS) was prepared via the polycondensation of 1,5-dichloranthraquinone with sodium sulfide, showing a reversible redox reaction at 2.33 V versus Li/Li^+ (50). Deng et al. (51) presented an all-organic battery with PAQS as the anode and poly(triphenylamine) (PTPAn) as the cathode. To improve the specific capacity and discharge voltage of PQs, Song et al. (52) synthesized poly(benzoquinonyl sulfide) (PBQS) with a smaller aromatic nucleus than PAQS. The PBQS cathode exhibited a high discharge voltage of 2.7 V versus Li/Li^+, high energy density of 734 Wh/kg, and stable long-term cycling (1,000 cycles, 86% retention). Moving to the very extended π-conjugated core as one route to improve kinetics, poly(pentacenetetrone sulfide) (PPTS) resulted in remarkable stability at a very high rate of 50 A/g, corresponding to a full charge in 7 s (53). The PPTS cathode chemistry was also proven functional for potassium-ion batteries (54).

Past work has also shown the efficacy of creating lithiated polymer salts to prevent dissolution (e.g., Li_2PDHBQS, LiDHAQS, and lithiated LNFP) (55–57). Other promising routes include quinoidic structures with thiophene rings or 1,4-dithiane, such as PVBDT, PBDTD, PBDTDS, and PDB (58–60). Also, polymers from biologically based cores such as dopamine and catechols have been proposed (e.g., PDA) (61, 62). PQs based on naphthotriazolediones (pNTQS) and

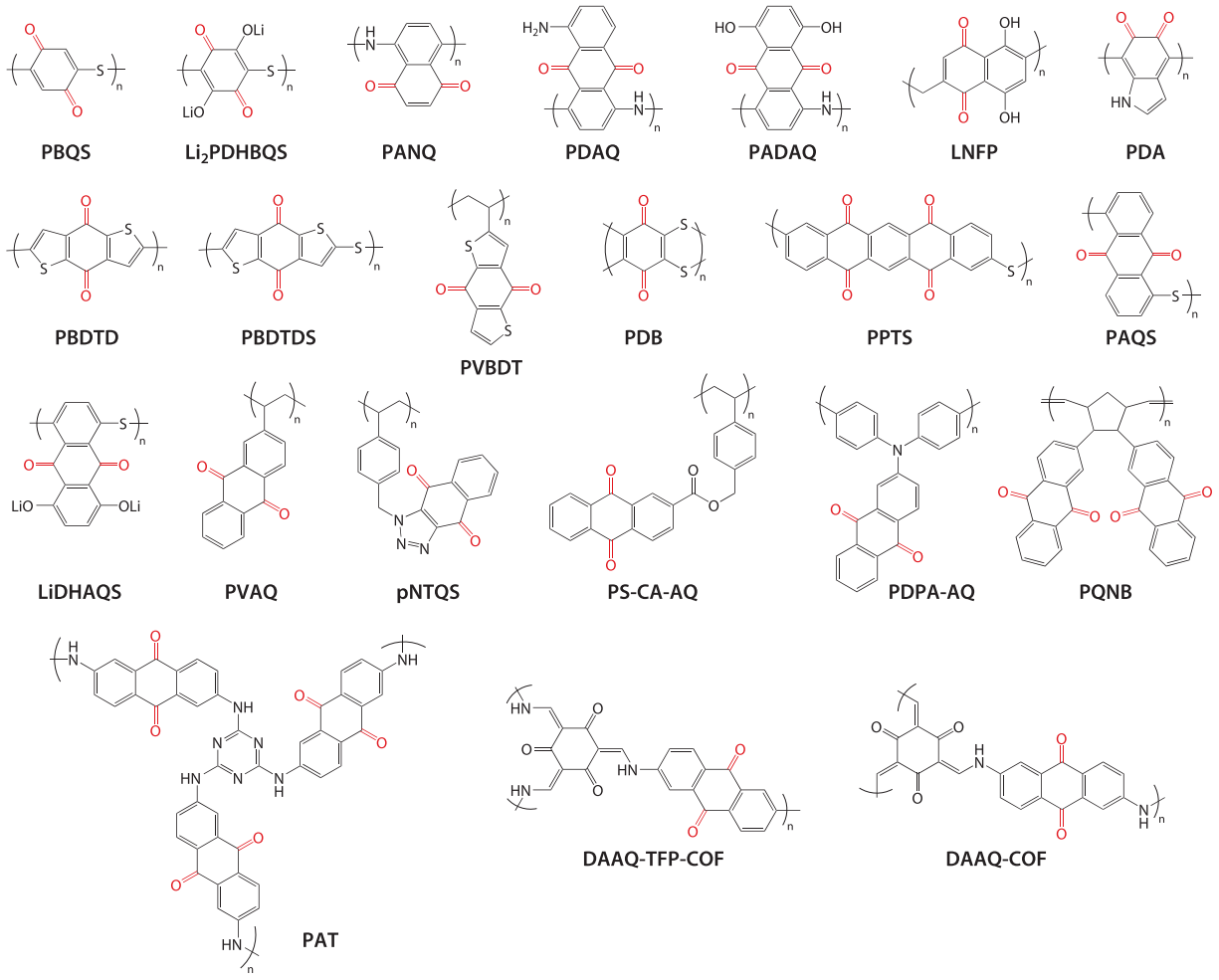

Figure 4

Molecular structures of representative polyquinones.

triphenylamine-anthraquinone (PDPA-AQ) pendant groups have also shown exceptional promise and stability (63, 64). Further, various polymers with quinones as the pendant group have additionally been explored, exhibiting competitive rate capability and cycling stability (e.g., PVAQ, PQNB, PS-CA-AQ) (65–67).

An emerging class of quinone-containing covalent organic frameworks (COFs) have unique advantages over traditional linear polymers, specifically fast charge transfer, fast proton conduction, and buffering against volume expansion (68–70). A 2,6-diaminoanthraquinone (DAAQ)-based COF nanosheet with a thickness of 5 nm delivered a much higher rate capability and cycling stability than the unexfoliated bulk sample (DAAQ-TFP-COF) (68). Kang et al. (70) synthesized polyanthraquinone-triazine (PAT) as an anode in lithium-ion batteries. This electrode enabled fast electron transport and complex Li^+ storage chemistry that combined a 17-electron redox reaction with a theoretical specific capacity of 1,450 mAh/g, showing high reversible capacities of 1,770 mAh/g at 200 mA/g. Gu et al. (69) synthesized a β-ketoenamine-linked DAAQ-COF

using 1,3,5-triformylphloroglucinol (TFP) and DAAQ as monomers. The resultant DAAQ-COF possessed abundant sodium storage sites (14 Na^+).

3.1.2. Polyimides. Polyimides (PIs) are known as important engineering plastics with high thermal stability and good mechanical strength and can be obtained by a simple one-step polymerization of a dianhydride as the redox-active unit and diamine or triamine as a connector. Theoretically, PIs can undergo two distinct reversible redox processes involving the transfer of two electrons in each. However, only one redox process is reversible in practice. The second redox process usually occurs at low potential and leads to structural degradation of the redox-active center due to repulsion between charges injected into the conjugated core.

Supplemental Material >

Several different PIs have been studied as active materials in rechargeable batteries, as shown in **Figure 5** and **Supplemental Table 3**. Early studies were carried out by Torres & Fox (71) in 1990 and Song et al. (72) and Oyaizu et al. (73) in 2010. Torres & Fox (71) showed that poly(*N*-3-thenylphthalimide) was electrochemically active at a more anodic potential than polythiophene and exhibited a conductivity of $2 \times 10^{-4}\ \Omega^{-1}\ cm^{-1}$ in the oxidized state. Oyaizu et al. (73) reported that pyromellitic dianhydride or 4,4′-oxydiphthalic anhydride (ODPA) can be connected to 1,4-phenylenediamine via polycondensation. The obtained PI electrodes (PMI-Ph, PODPA-Ph) showed severe capacity decay due to dissolution. In contrast, naphthalene-based (1,4,5,8-naphthalenetetracarboxylic dianhydride, NTCDA) and perylene-based (3,4,9,10-tetracarboxylic dianhydride, PTCDA) PIs with large π-conjugated redox groups have higher molecular weight, leading to a reduced specific capacity but improved cycling stability and discharge voltages (e.g., PMI-Ph, PMI-12, NDI-Ph, NDI-Hy, NDI-12, PAQI-N26, PAQI-B26 and PDI-12, PDI-Hy) (72, 74, 75). This is because the large π-conjugated core yields delocalized scaffolds to promote charge compensation and structural stability of the reduced state.

Also, structural configuration significantly affects PI electrochemical performance. Xu et al. (76) compared two isomeric PAQIs, indicating that so-called 14 isomers (PAQI-B14, PAQI-N14) had lower overpotentials, higher discharge capacities, higher cyclabilities, and better rate capabilities than "15" isomers. It was shown elsewhere that PIs with urea help to promote electron sharing in the structure, which then enhances the electrical conductivity (e.g., NOP, POP) (77, 78). To further improve PI's electrical conductivity, a π-conjugated PI was synthesized from bithiophene associating with the π-core of naphthalene diimide (NDI) (79). The obtained P(NDI2OD-T2) exhibited higher electrical conductivity due to the conjugated skeleton as compared with P(NDI2OD-TET), which exhibited more nonconjugated character.

PI-based COFs have shown promise for addressing ion diffusion limitations (80–82). By moving to 2D PIs, ion diffusion may be improved even further. Tian et al. (83) synthesized three 2D PIs (PMI-TAPB, NDI-TAPB, PDI-TAPB) by condensation; although the obtained PIs showed non-ideal battery performance, the higher surface area and microporosity of PMI-TAPB improved ion mobility. Elsewhere, a 3D skeleton structure reported by Schon et al. (84) promoted the transport of ions (e.g., PDI-Tc).

3.1.3. Polyketones. Unlike PIs, polyketones can adopt four-electron redox reactions, suggesting a higher theoretical capacity. **Figure 6** and **Supplemental Table 4** show representative polyketones and the corresponding electrochemical properties. Geng et al. (85) synthesized a polyketone consisting of *N*,*N*′-diallyl-2,3,5,6-tetraketopiperazine (o-AP) units with four carbonyl groups in an *N*-cyclic structure. However, o-AP exhibited poor cycling stability due to its solubility in organic electrolytes, and an irreversible structural change was triggered when accessing the full four-electron redox reaction. To promote the stability of ketone groups in organic electrolytes, cyclic 1,2-diketone units were grafted to the polymethacrylate backbone to form a copolymer-bound pyrene-4,5,9,10-tetraone (PPYT) (86). PPYT delivered a practical capacity of 231 mAh/g

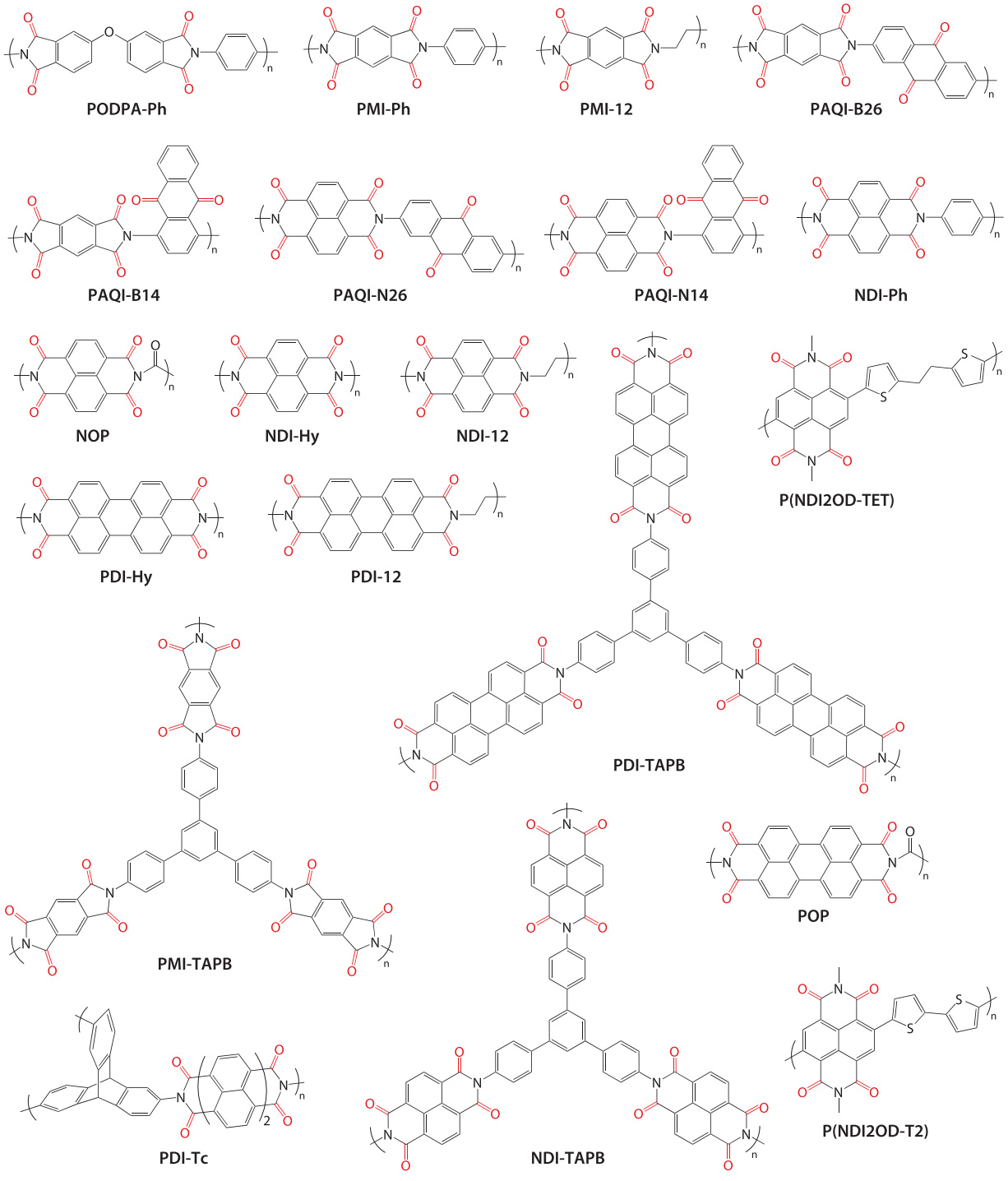

Figure 5

Molecular structures of representative polyimides.

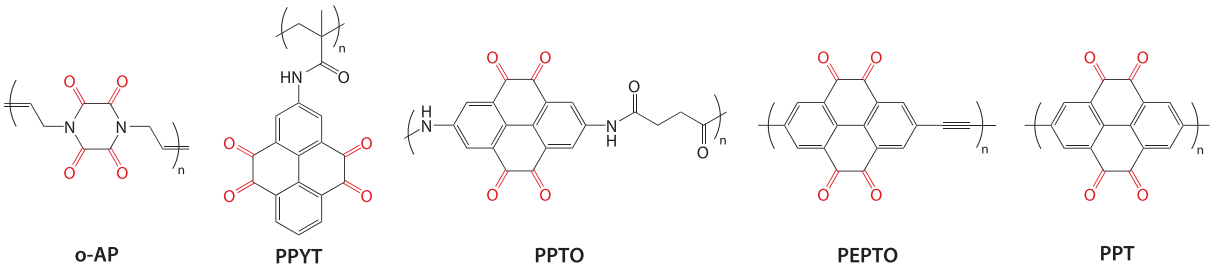

Figure 6

Molecular structures of representative polyketones.

at 0.2 C and a capacity retention of 83% after 500 cycles at 1 C. Liang et al. (87) synthesized a polyketone with pyrene-4,5,9,10-tetraone (PTO) as the redox-active pendant group and employed PPTO as an anode material in aqueous batteries. In neutral 2.5 M Li_2SO_4 aqueous electrolyte, PPTO achieved 92 Wh/kg when paired with $LiMn_2O_4$ cathode at an average voltage of 1.13 V. This performance is in the same range as the competing system $LiTi_2(PO_4)_3$-$LiMn_2O_4$ (90 Wh/kg) owing to the extremely high capacity of the PPTO electrode (229 mAh/g at 1 C). More recently, poly(2,7-ethynylpyrene-4,5,9,10-tetraone) (PEPTO) and poly(pyrene-4,5,9,10-tetraone) (PPT) were developed as cathodes in lithium batteries (88, 89) and sodium batteries (90). The replacement of a single C–C bond (in PPT) with a carbon–carbon triple bond (in PEPTO) greatly enhanced electrode performance (88). The above investigations indicate that polyketones have great potential as electrode materials for batteries through the rational design of chain structures.

3.1.4. Sulfur-based polymers. One additional functional group that can be leveraged for NC-RAPs is sulfur-based groups, such as disulfides and thioethers, summarized in **Figure 7** and **Supplemental Table 5**. The general redox reaction for sulfur-based groups is the cleavage (reduction) and formation (oxidation) of the disulfide (S–S) bond. For example, Trofimov et al. (91) presented the synthesis and electrochemical characterization for a family of polyeneoligosulfide (PES) cathodes that exhibited initial capacities of 720 mAh/g, but with severe capacity fade due to the dissolution of polysulfide sulfur from the electrode. In contrast, Sarukawa & Oyama (92) demonstrated a sulfur-linked tetrathionaphthalene polymer (PS-TTN) electrode that exhibited a lower discharge capacity of 122 mAh/g with an excellent capacity retention of 90% after 180 cycles. Su et al. (93) studied a composite electrode using polyaniline derivative with disulfide bonds (PAPOD) as the active material with an initial capacity of 230 mAh/g but with significant capacity fade after only 7 cycles. To address the stability and dissolution issues associated with the discussed organosulfur polymers, Pyun and colleagues (94) proposed inverse-vulcanized polymers (PS-r-DIB); these polymers used a divinyl benzene unit crosslinked with elemental sulfur, leading to high charge capacities, enhanced capacity retention, and improved rate capabilities. To improve upon the inverse-vulcanized polymers, Grocke et al. (95) studied crosslinked disulfide polymers to improve the reversibility of the redox reaction as compared to small-molecule disulfides and previous polymeric systems.

Supplemental Material >

3.2. P-Type NC-RAPs

Similar to cation-compensated nonconjugated redox-active polymers, anions (negatively charged ions) instead of cations are introduced into the polymer matrix to compensate for the charge imbalance caused by the presence of redox-active groups. Here we discuss examples of p-type polymers.

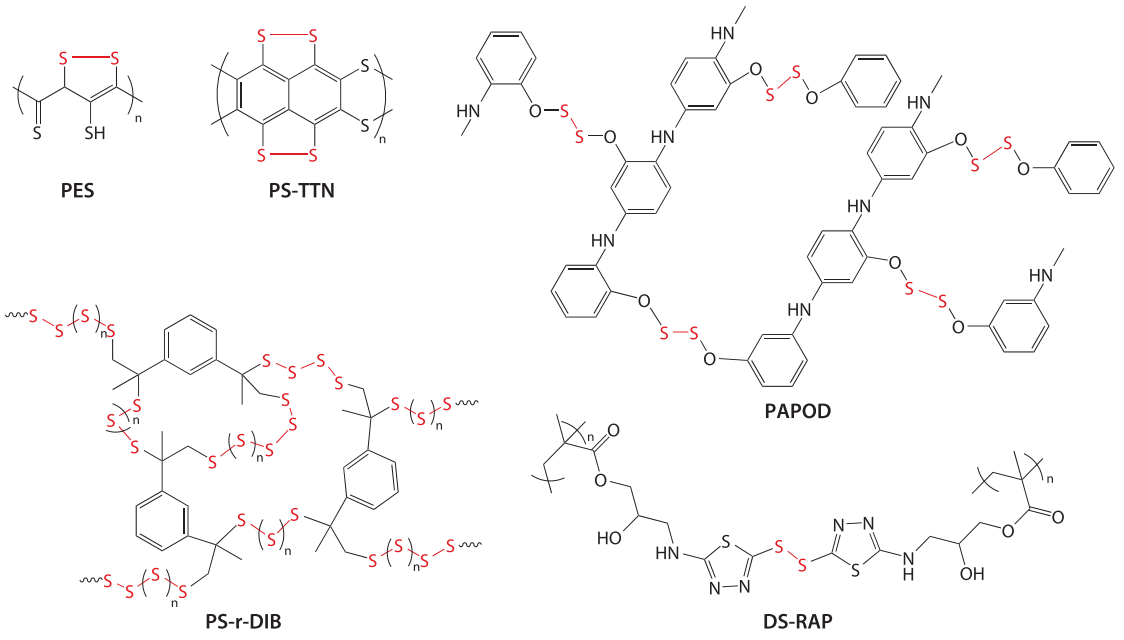

Figure 7

Chemical structures of the presented polymers.

3.2.1. Radical-containing polymers. Radical-containing polymers generally consist of an insulating polymer backbone and stable pendant radicals such as TEMPO, nitronyl nitroxide, 2,2,5,5-tetramethylpyrrolidin-*N*-oxyl (PROXYL), or verdazyls, as shown in **Figure 8** and **Supplemental Table 6**.

Supplemental Material >

Of all TEMPO-containing radical polymers, poly(TEMPO-methacrylate) (PTMA) is the most well-known, because it is easy to synthesize, is stable in air and water, and exhibits a near-theoretical specific capacity of 111 mAh/g (96). Wang et al. (97) showed a quantitative view of in situ ion transport and doping in PTMA during the redox process by in situ electrochemical quartz crystal microbalance with dissipation monitoring (EQCM-D). Considering the dissolution issue of PTMA, Wang et al. (98) synthesized crosslinked PTMA-*co*-glycidyl methacrylate (PTMA-GMA) via a simple post-synthesis crosslinking technique. Qin et al. (99) synthesized crosslinkable TEMPO-containing branched polymer. Elsewhere, PTMA was grafted onto surface initiator–modified indium tin oxide (ITO) substrates to create a covalent bond between PTMA and ITO to prevent PTMA dissolution (100).

PTMA tacticity was also reported to influence its redox potential and reversibility. López-Peña et al. (101) reported that PTMA synthesized by group transfer polymerization revealed two distinct redox processes, of which one proved to be reversible and another irreversible. The reversible process was ascribed to the redox reaction of the TEMPO moieties from isotactic domains in the polymer. The irreversible process was linked to smaller heterotactic and syndiotactic domains in the PTMA polymer. Except the commonly used aminoxyl radical/oxoammonium cation redox process, the TEMPO scaffold itself can also be reduced to the corresponding aminoxy anion. This reduction process is normally considered to be irreversible, but it can be stabilized when TEMPO is polymerized and embedded in graphite or cellulose; this yields an even higher specific capacity of 222 mAh/g (102, 103). Elsewhere, Nesvadba et al. (104) synthesized a spirobisnitroxide polymer

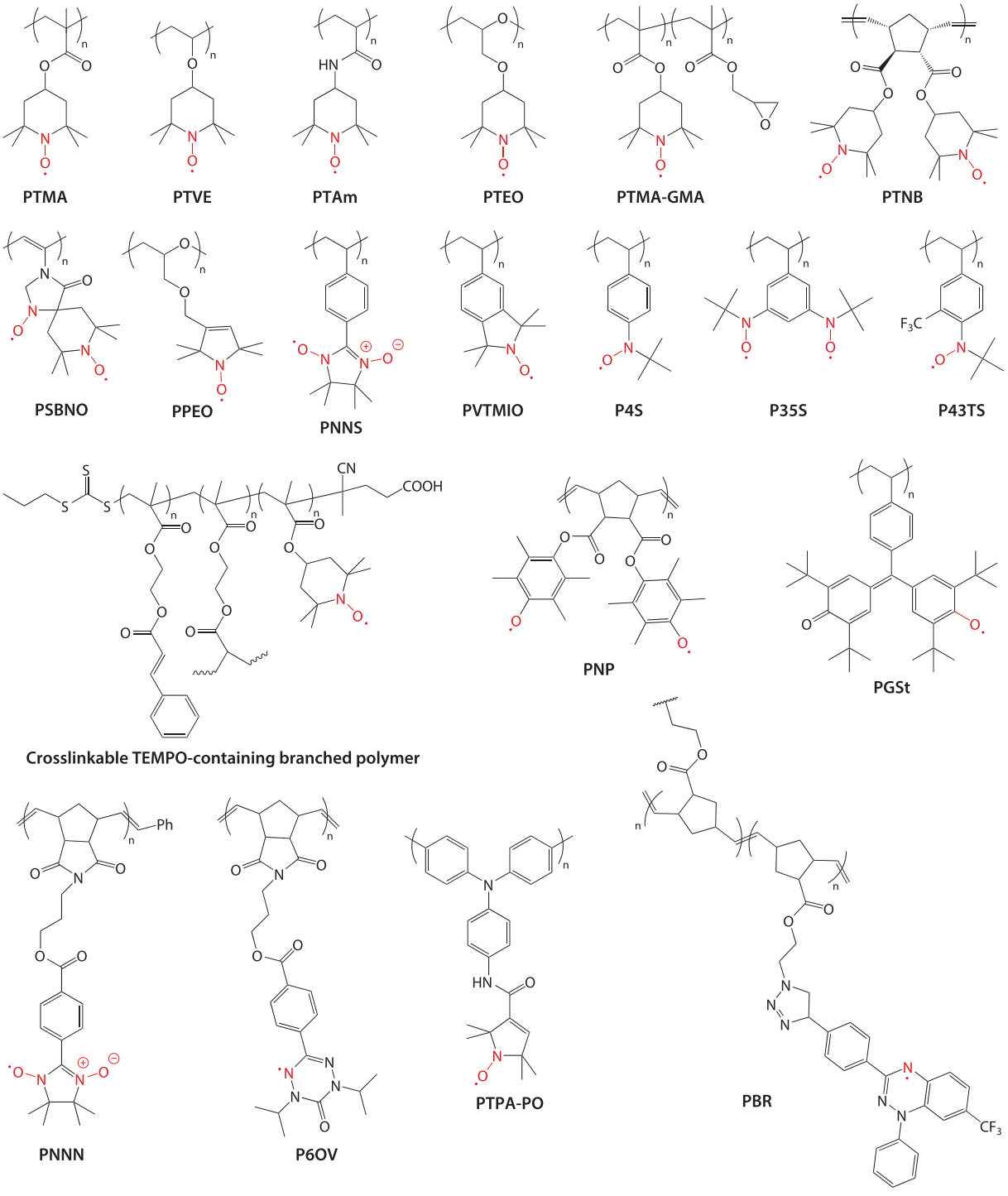

Figure 8

Representative radical-containing polymers.

(PSBNO) with two electrochemically different nitroxide groups to yield a very high theoretical capacity of 174 mAh/g.

Usually, the backbone of PTMA shows low electrical conductivity. However, Boudouris and colleagues (43) reported that PTEO exhibited excellent conductivities up to 28 S/m. The flexible and ionophoric polyether backbone allowed for efficient charge propagation within the polymer, which can lead to efficient charging–discharging characteristics and high discharge currents without substantial loss of output voltages (PTEO, PPEO) (26, 105).

Other types of radical polymers have also been investigated as solid-state, redox-active materials. Verdazylic compounds display a reversible redox process and have been introduced into a polynorbornene backbone by Gilroy, Anghel, and colleagues (106). An aliphatic linker was used to connect the verdazylic group to norbornene dicarbonimide, which was later polymerized via radical-tolerant ring-opening metathesis polymerization using a Grubbs catalyst (P6OV) (107). The compound exhibited an amphoteric behavior by showing a reduction reaction at −0.96 V and an oxidation reaction at 0.49 V versus ferrocene. Following a similar strategy, a nitronyl nitroxide polymer was obtained by linking the redox-active unit to a polynorbornene backbone via a ring-opening metathesis polymerization (PNNN) (106). In another approach, Hansen et al. (108) synthesized poly(5-vinyl-1,1,3,3-tetramethylisoindolin-2-yloxyl) (PVTMIO) and used it as a cathode in a lithium battery. The obtained polymer exhibited an oxidation potential of 3.7 V versus Li/Li^+ and delivered a capacity of 104.7 mAh/g.

Nitroxide radical chemistry has also been used in organic polymer batteries. Specifically, a bipolar radical battery, using poly(nitronylnitroxylstyrene) (PNNS) as anode and poly(galvinoxylstyrene) (PGSt) as cathode material, yielded a capacity of 44 mAh/g and a lifetime of more than 250 cycles at a working voltage of 1.3 V (109). In another study, Xiong et al. (110) linked a 2,2,5,5-tetramethyl-1-pyrrolidinyloxy (didehydro-PROXYL) radical to a triphenylamine polymer (PTPA-PO), which was then oxidatively polymerized using $FeCl_3$. The polymer electrode exhibited two voltage plateaus at 3.7 V and 2.7 V (versus Li/Li^+) corresponding to the reaction of PROXYL and triphenylamine. A capacity of 120 mAh/g was obtained, decreasing by 10% after 100 cycles at various charging rates. Furthermore, Schubert and coworkers (111) investigated radical polymers based on phenoxyl-radical compounds (PNP). The redox-active units were introduced as side groups to a polynorbornene backbone. The corresponding battery tests showed a capacity of 60 mAh/g and a 20% loss after 100 cycles. Recently, Saal et al. (112) investigated polymeric Blatter radical (PBR) as a cathode material and reported a capacity of 33 mAh/g, which is 76% of the theoretical capacity (45.9 mAh/g).

Electrolyte design is also an important parameter to optimize the performance of radical polymer-based electrodes. Using an aqueous electrolyte, Ma et al. (32) explored three different TEMPO-based NC-RAPs (PTMA, PTVE, PTAm), showing that the kinetics and performance increased for NC-RAPs with more favorable polymer–water interactions. Specifically, hydrophilic backbones promote charge transfer kinetics and, therefore, capacity. This is because electrolyte penetration was promoted (but not so much as to cause dissolution). Gerlach et al. (113) investigated the effect of salt concentration on the electrochemical performance of PTMA composite electrodes with 1-butyl-1-methylpyrrolidinium tetrafluoroborate (Pyr_14BF_4) in propylene carbonate as electrolyte. As the electrolyte concentration increased, the capacity decreased due to the electrolyte's higher viscosity. Previously, our group also investigated the Hildebrand and Hansen solubility parameters, which can be used to select suitable casting solvents and electrode additives (114).

3.2.2. Polyphenylamines. Polytriphenylamine (PTPA) and its derivatives are other stable radical polymers of interest due to their excellent charge transport and thermal stabilities. Feng

et al. (115) reported PTPA as a cathode material with a discharge capacity of 90 mAh/g at 20 C after 1,000 cycles with nearly 100% coulombic efficiency. The fast charge transfer process occurred because the redox centers were stabilized by a conjugated backbone, allowing for partial charge delocalization. Su et al. (116) synthesized a similar phenylamine polymer, poly(*N*,*N*,*N*,*N*-tetraphenylphenylenediamine) (PDDP), with an initial discharge capacity of 129 mAh/g in 0.1 M lithium perchlorate in acetonitrile. The improved capacity and rate capability were ascribed to the higher radical density as compared to PTPA. Obrezkov et al. (117) inspected poly(*N*,*N*′-diphenyl-p-phenylenediamine) (PDPPD), for ultrafast Li-, Na-, and K-ion batteries. They reported a discharge capacity of 94 mAh/g at 10 C with a capacity retention of 67% after 5,000 cycles in 1 M $LiPF_6$ in ethylene carbonate (EC)/dimethyl carbonate (DMC).

3.2.3. Polyphenazines. Polyphenazines (PNZs) are a class of polymers with heterocyclic nitrogen-containing molecules displaying excellent electrochemical performance. The presence of less hydrophilic groups in the peripheral of PNZ makes it insoluble in water, resulting in excellent cycling stability in aqueous electrolytes. Obrezkov et al. (118) investigated poly(*N*-phenyl-5,10-dihydrophenazine) (p-DPPZ) for cathodes, revealing an energy density of 564 mWh/g and discharge capacity of 162 mAh/g at 1 C with 2.2 M KPF_6/diglyme solution as the electrolyte. Lee et al. (119) investigated *N*,*N*′-substituted phenazine (NSPZ) showing multi-electron reaction with specific energy of 622 mWh/g in dual-ion batteries.

3.2.4. Polyphenothiazines. Polyphenothiazines (PTZs) are organic compounds like PNZ with N and S atoms present in the core ring structure, as shown in **Figure 9** and **Supplemental Table 7**. Kolek, Otteny, and colleagues (120, 121) employed poly(3-vinyl-*N*-methyl phenothiazine) (PVMPT) as the cathode, exhibiting a high cycling stability due to the π-π interactions of the phenothiazine side groups. Reducing the mobility of the PVMPT redox polymer in the battery electrode through crosslinking also significantly improved the cycling stability (X-PVMPT) (122). Elsewhere, Schmidt et al. (123) synthesized calix[n]phenothiazines. Peterson et al. (124) investigated poly(*N*-methylphenothiazine dimethylphenylenediamine) (PT-DMPD) and poly(*N*-methylphenothiazine benzidine) (PT-BZ) synthesized by copolymerization of *N*-methylphenothiazine with electron-rich and redox-active aryl diamines units. They reported a discharge capacity of 128 mAh/g and 97 mAh/g for PT-DMPD and PT-BZ, respectively, in 1 M $LiPF_6$ in EC/DEC. However, both the polymer electrodes have a low coulombic efficiency (35% for PT-DMPD and 48% for PT-BZ) due to the dissolution of polymer in its oxidation state. Then, PT-DMPD was crosslinked to avoid dissolution, exhibiting a discharge capacity of 150 mAh/g with an improved coulombic efficiency of 82%. Elsewhere, Kuzin et al. (125) investigated the electrode kinetics and electropolymerization conditions of two phenothiazine derivatives, 3,7-bis(4-aminophenylamino) phenothiazin-5-ium chloride (PhTz-$(NH_2)_2$) and 3,7-bis(4-carboxyphenylamino) phenothiazin-5-ium chloride (PhTz-$(COOH)_2$).

3.2.5. Polyphenoxazines. Phenoxazines (PXZs) are organic compounds that have an oxygen atom instead of the sulfur in PTZs. Unlike PTZs, PXZs have a planar conformation in the neutral and radical cation state, which promotes fast charge transfer. Otteny et al. (126) replaced the sulfur atom with an oxygen atom and synthesized linear (PVMPO) and crosslinked (X-PVMPO) PXZ-based polymers as the cathode, affecting the interactions within the polymer as well as the electrochemical properties.

3.2.6. Polythianthrene. Polythianthrenes have sulphur-containing heterocycles. They can sustain a stable radical cation form upon oxidation and can be used for high-voltage organic cathode materials. Speer et al. (127) investigated three thianthrene-functionalized polynorbornenes

Supplemental Material >

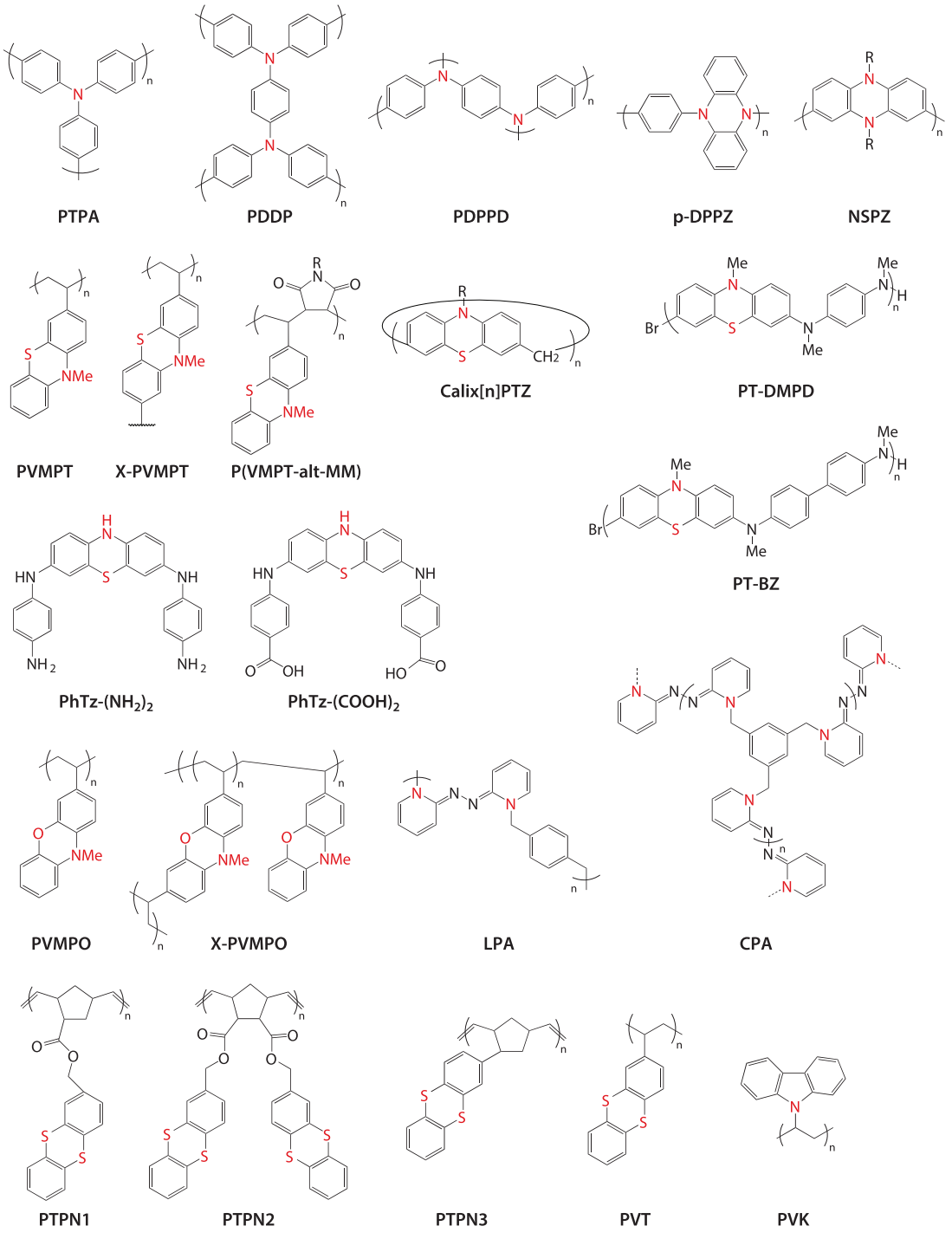

Figure 9

Other representative nonconjugated redox-active polymers.

(PTPN1, PTPN2, PTPN3) with an average high discharge potential of 4.1 V versus Li/Li$^+$. Wild et al. (128) employed poly-(2-vinylthianthrene) (PVT) as cathode for an all-polymer battery, exhibiting an initial discharge capacity of 105 mAh/g with a discharge voltage of 1.35 V.

3.2.7. Polyazine. Polyazines are N-N linked diamine-based polymers and can undergo two reversible redox reactions, making azine an alternative battery cathode material. Acker et al. (129) reported linear (LPA) and crosslinked (CPA) azine-based polymers as the cathode with two electron reactions at 2.9 V and 3.3 V versus Li/Li$^+$. The end-capped crosslinked azine-based polymers displayed an excellent cyclic stability with an initial discharge capacity of 133.4 mAh/g and high-rate performance up to 100 C. After 200 cycles, 85% of the capacity was retained with almost 100% coulombic efficiency.

3.2.8. Polyvinyl carbazole. Among the pendant-type polymers, polyvinyl carbazole (PVK) has been studied for its application as a positive electrode for lithium-ion batteries because of its redox potential of 1 V versus NHE (130). The π-stacked carbazole group in PVK is attached to an insulating aliphatic chain. This forms the electronic pathway, giving a theoretical capacity of 138 mAh/g. Yao et al. (131) described electrochemical crosslinking of PVK. They observed that the 3 and 6 positions of the cation radical cause the coupling reaction between the nearby carbazole moieties, resulting in polymer crosslinking.

3.2.9. Polyviologens. Viologen-based polymers exhibit a unique reversible two-electron redox mechanism that occurs in two steps. In the first step, at higher potentials, viologen is reduced from a dication to a radical cation state. In the second step, at lower potentials, the radical cation is reduced further to the neutral viologen. **Figure 10** and **Supplemental Table 8** show select examples of viologens from the literature. Sano et al. (132) provided one of the most impactful demonstrations of viologen-based electrodes, using electropolymerization to produce a fully crosslinked electrode to prevent dissolution. The viologen-based electrode (PTPM) exhibited a capacity of 174 mAh/g with a high coulombic efficiency in an aqueous electrolyte. Additionally, they demonstrated a fully polymeric battery, with a nitroxide-based cathode, that resulted in an output potential of 1.14 and 1.52 V with a capacity of 165 mAh/g (132). Beladi-Mousavi et al. (133) subsequently used various viologen-based polymers (PV1–4) that were self-assembled with graphene oxide, resulting in a maximum capacity of 216 mAh/g.

Supplemental Material >

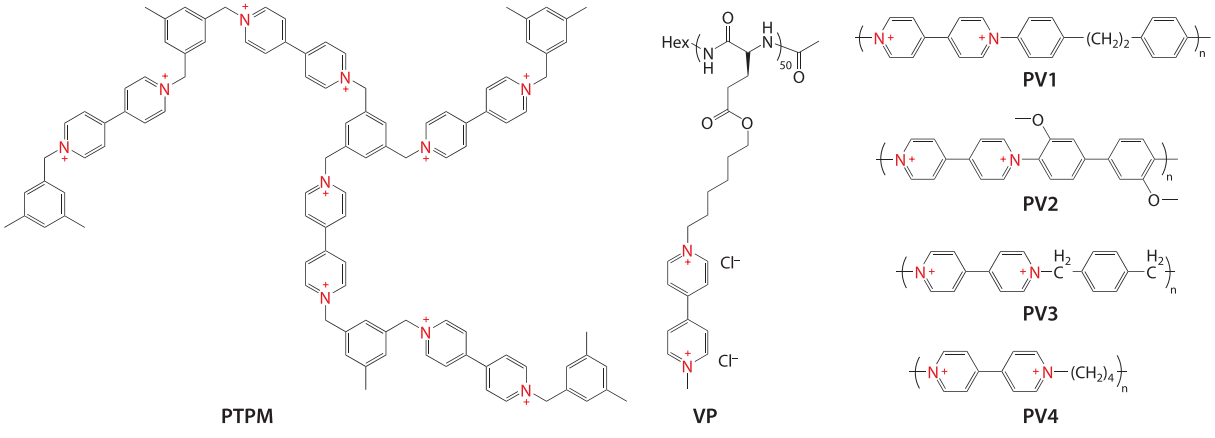

Figure 10

Representative polyviologens.

Nguyen et al. (134) demonstrated the use of a viologen-based polypeptide (VP) as an anode material and TEMPO-based polypeptide cathode material in a fully polymeric battery, in which the polymers adopted alpha-helix conformations. The VP anode exhibited a capacity of 74.2 mAh/g, and the polypeptide could be deconstructed after use to regenerate the glutamic acid backbone and viologen derivatives (134). This study showed the promise of deconstructable batteries, but the viologen group should be replaced in future applications due to environmental considerations.

3.3. Ambipolar NC-RAPs

In addition to the cation- and anion-exchanging polymers discussed above, bipolar/ambipolar polymers can be both reduced and oxidized to be compensated by both cations and anions, respectively. The ambipolar chemistry allows one to use the same material as both cathode and anode, or use the material over its full redox range to improve its capacity. Currently, there are two main approaches in the literature to produce ambipolar polymers: (*a*) Include both p-type and n-type redox active groups in each repeat unit, and (*b*) include a single ambipolar redox group on each repeat unit (**Figure 1**). **Figure 11** and **Supplemental Table 9** summarize ambipolar structure and performance.

Supplemental Material >

The first type, in which both n-type and p-type groups are incorporated, typically suffers from internal charge transfer between the two redox active groups, manifesting as poor coulombic efficiencies at low charge/discharge currents and self-discharge. This challenge is similar to that faced with conjugated radical polymers with mismatched redox potentials (135).

As an alternative approach, n-type and p-type redox-active groups can be merged into a singular unit. Wang et al. (136) demonstrated an in situ electropolymerizable amino-phenyl carbazole naphthalene diimide (ACPCNDI) with ambipolar redox behavior and an initial capacity of 141 mAh/g (71% theoretical) at 0.1 A/g. The naphthalene diimide unit was responsible for

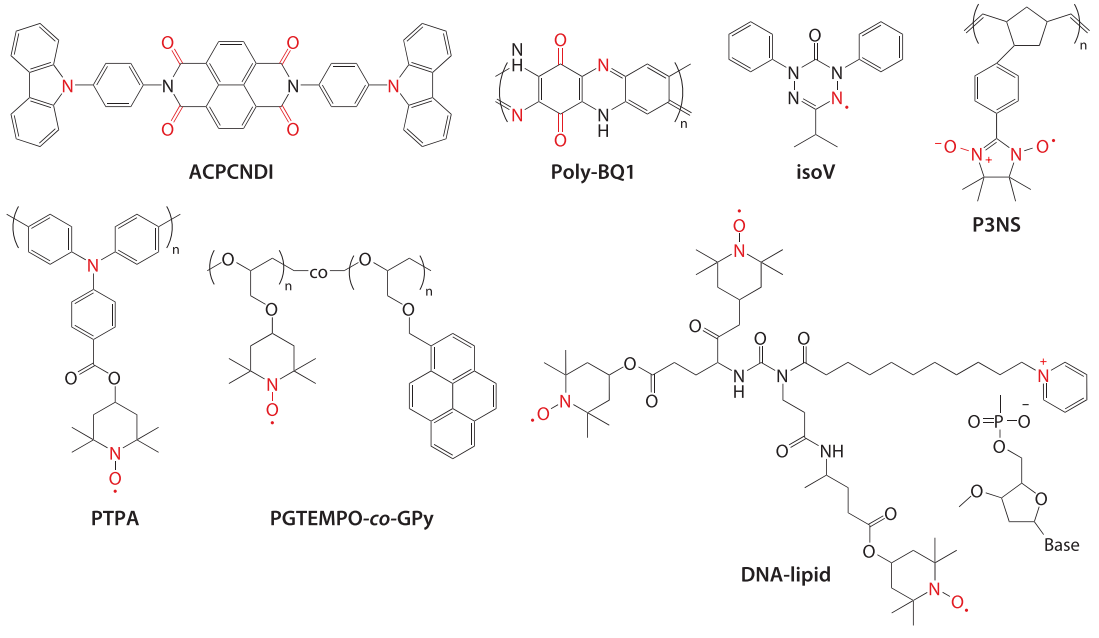

Figure 11

Select ambipolar redox-active polymers.

the n-type reaction, whereas the carbazole unit imparted the p-type reaction for the demonstrated polymer (136). Elsewhere, Zhao et al. (137) synthesized a polymer (Poly-BQ1) that contained benzoquinone and diimine units exhibiting a capacity of 351.5 mAh/g, whereas Xie et al. (60) used quinone and dithioether units (PDB), resulting in a capacity of 249 mAh/g (78% of theoretical). Other examples include phenothiazine with naphthalene-based PIs (60, 138), PTMA-anthraquinone copolymers (139), and a benzoquinone–diimide–pyrazine polymer (140).

The second approach, in which a single ambipolar redox group is used, suffers less from internal charge transfer then the first approach described above. The most common ambipolar redox-active groups in the literature are nitroxide radical-based functional groups, including TEMPO, nitronylnitroxide, and nitroxylstyrene.

One of the most prominent functional groups found in the literature for pendant redox-active polymers is TEMPO, which is most used as a cathode. However, TEMPO can also be reduced (in an n-type reaction) to form the aminoxy anion. This additional reaction has been used to develop electrodes of greater accessible capacity, compared to those accessing only the p-type reaction (141). Qu et al. (142) demonstrated the ambipolar redox behavior for TEMPO-containing DNA complexes (DNA-lipid), which exhibited a maximum capacity of 60 mAh/g (96% of theoretical) when composited with carbon fiber (80 wt%) and PTFE binder (10 wt%). Others have since studied the ambipolar redox behavior for PTMA–graphene–Ketjen black composites (143, 144), PTMA-grafted carbon nanotubes (145), PTMA–pyrene copolymers (PGTEMPO-*co*-GPy) (141), TEMPO-functionalized polypeptides (146), and TEMPO-functionalized PTPA (147) (**Figure 11**). Besides PTMA, Deng et al. (41) presented the bipolar energy storage for PTEO-based composite electrodes, which exhibited a capacity of 220 mAh/g (92% of theoretical) when composited with only 30 wt% SuperP carbon black and 10% of PTFE.

Another commonly used nitroxide-based redox-active group is nitronylnitroxyl (NN), which can undergo similar oxidation and reduction reactions as TEMPO. The n-type reaction associated with the reduction from the nitroxide radical to the aminoxyl anion has been characteristic for NN-based electrodes in the literature. Suga et al. (109) first demonstrated the use of PNNS as both the anode and cathode active materials, resulting in a battery with a maximum capacity of 44 mAh/g (86% of theoretical) with vapor-grown carbon fiber (80 wt%) and polyvinylidenefluoride resin (10 wt%). Sukegawa et al. (148) changed the backbone of PNNS to a poly(norbornene) (P3NS), which resulted in a charge capacity of 67 mAh/g (82% of theoretical capacity) for the p-type reaction and 52 mAh/g (63% theoretical) for the n-type reaction. Anghel et al. (106) presented the synthesis of a similar NN polymer; however, they did not observe a reversible n-type/reduction reaction in solution state. Additionally, Suga et al. (149) demonstrated that substitution of trifluoromethyl at the ortho position in poly(nitroxylstyrene) changed the redox mechanism to prefer the n-type reaction of the nitroxide, whereas the p-type reaction was observed for the unsubstituted nitroxylstyrene. Jähnert et al. (150) also observed changes in redox mechanism with substituted poly(nitroxylstyrene).

Another ambipolar group of interest is the verdazyl group. Anghel et al. (106), Paquette et al. (151), and Price et al. (152) demonstrated the solution-state ambipolar behavior of a polymer with 6-oxoverdazyl. Magnan et al. (153) presented different substitutions on the verdazyl ring (isoV) to change the solution-state potential of the n-type and p-type reactions and the resulting cell voltage.

Looking forward, some examples of solution-state ambipolar redox behavior show promise as future polymer-based electrodes, some of which have been reviewed elsewhere (154). For example, Saal et al. (112) demonstrated the ambipolar behavior of polymers containing 1,2,4-benzotriazinyl radical (Blatter radical). Future work should focus on ambipolar groups with greater stability and larger voltage differences for the n-type and p-type reactions (155, 156).

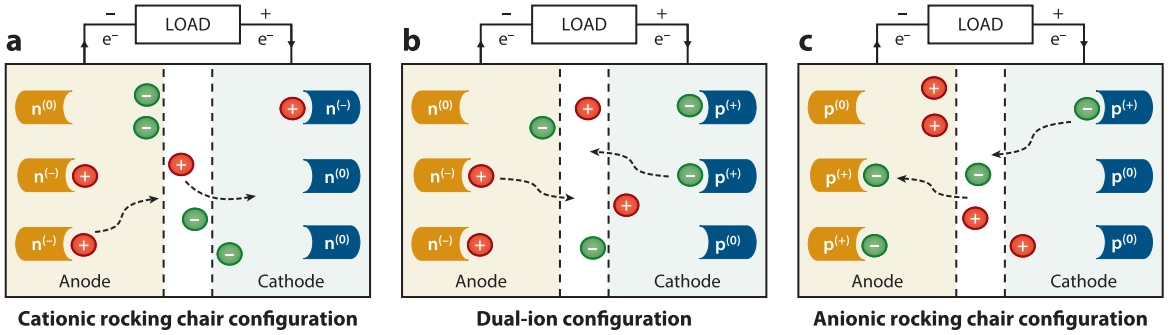

Figure 12

Schematics for different cell configurations with n-type and p-type polymers during charge–discharge operations.

4. CELL DESIGN CONSIDERATIONS

4.1. Cell Configuration

From the previous section, we know NC-RAPs can be classified into p-type, n-type, and ambipolar polymers, depending on whether the NC-RAP exchanges cations, anions, or both, respectively (157). Given these choices, there are three main types of cell configuration: cation rocking chair, anion rocking chair, and dual ion (**Figure 12**).

4.1.1. Cation rocking chair. For this configuration, both the cathode and anode materials are typically n-type polymers in which the cation counterbalances the negative charge formed in the electrodes. Zhu et al. (158) used polyparaphenylene for both the cathode and anode in which Li ions were the charge carrier. Wang et al. (159) reported a 0.8 V proton rocking chair battery in which the proton exhibited a high diffusion coefficient. Quinizarin and naphthoquinone were covalently attached to terthiopene units to make cathodes and anodes, respectively, to yield a capacity of 62 mAh/g and a capacity retention of 80% after 500 cycles at 4.5 C.

4.1.2. Anion rocking chair. In this form, the cathode and anode contain p-type polymers in which anions counterbalance the positive charge. Yao et al. (160) demonstrated an anion rocking chair battery using PVK as the cathode and poly(1,1′-pentyl-4,4′-bipyridinium dihexafluorophosphate) as the anode. PF_6^- insertion and deinsertion took place during the charging and discharging process. Sano et al. (132) reported an all-organic battery with poly(2,2,6,6-tetramethylpiperidinyloxy-4-yl acrylamide) (PTAm) as the cathode and highly crosslinked polyviologen hydrogel as the anode material, cycling more than 2,000 times with compensating Cl^- anions. Elsewhere, Chikushi et al. (161) used PTAm as the cathode and poly(*N*-4,4′-bipyridinium-*N*-decamethylene dibromide) (PV)(10) as the anode with three different anionic species (Cl^-, BF_4^-, and PF_6^-). The PTAm|PV(10) cell reported a discharging capacity of 104 mAh/g with a coulombic efficiency of more than 95%. Recently, a polypeptide-based anion rocking chair battery was reported, in which viologens and nitroxide radicals were incorporated as redox-active groups along polypeptide backbones to function as anode and cathode materials, respectively (134).

4.1.3. Dual ion. In this configuration, a p-type polymer serves as cathode and an n-type polymer serves as anode. The potential advantages of dual-ion batteries are high working voltage, safety, and fast charging (162). However, ion concentration changes during dual-ion battery operation require high salt concentrations in the supporting electrolyte (4). During the charging process,

the reduced n-type polymer combines with cations, whereas the oxidized p-type accepts anions. During the discharge process, the cations and anions diffuse back to the electrolyte as the polymers return to their neutral state. Zhang et al. (163) reported a dual-ion battery based on PTMA and PI with NH_4SO_4 as the electrolyte. A discharge capacity of 136.5 mAh g^{-1} was reported for a current density of 0.5 A g^{-1} with a capacity retention of 86.4% after 10,000 cycles. Deng et al. (51) reported a Na-ion battery with poly(triphenylamine) as the cathode and PAQS as the anode; they reported a discharge potential of 1.8 V versus Na^+ with a specific capacity of 92 Wh/kg. Suga et al. (164) investigated poly[4-(*N-tert*-butyl-*N*-oxylamino)styrene] and poly[4-(*N-tert*-butyl-*N*-oxylamino)-3-trifluoromethylstyrene] as cathodes and anodes, respectively. While charging, nitroxide radicals in the cathode are oxidized to oxoammonium cations, whereas nitroxide radicals in the anode are reduced to aminoxy anion forms. Notably, the n-type nitroxide radical polymer contained the electron-withdrawing trifluoromethyl (CF_3) group to stabilize the aminoxy form.

5. CONCLUSION AND FUTURE OUTLOOK

NC-RAPs are promising materials for addressing challenges associated with energy storage. These materials offer the prospect of metal-free or low-metal energy storage, fast kinetics, and possibly circular batteries. NC-RAPs can exchange cations, anions, or both, leading to versatility in the cell design choice from cation and anion rocking chair cells to dual-ion cells. With the combined versatility in cell design and synthetic landscape, we envision a future in which NC-RAPs can be designed specifically for a targeted application.

The design of next-generation NC-RAPs should be bolstered by machine learning/artificial intelligence computing and materials genome science. The vast synthetic landscape afforded by the near-limitless combinations of backbones and redox cores cannot be explored efficiently with a trial-and-error approach. Few have begun to combine computational exploration with experiment. One notable example that points to a way forward is from Tan et al. (165), who examined molecular design features in NC-RAPs for the purposes of charge transfer in the solid state for interpretation of electrical conductivity. Another notable example is from Li & Tabor (156), who used machine learning to identify low-potential radical cores for use in organic polymers batteries. Taken together, these approaches could reduce experimental exploration and time while providing fundamental understanding of major factors contributing to redox potential and charge transfer kinetics.

On the practical side, NC-RAPs still require large improvements in specific energy, which is related to the product of the voltage and capacity. Accordingly, it is desirable to create a battery with a large cell voltage, but both p-type and n-type polymers are challenged by their poor stability at extremely oxidizing or reducing potentials. Synthetic and physical chemists thus face an immense opportunity, whereby the charge can be stabilized by electron-donating/-withdrawing chemistries and proper electrolyte design. For example, Yan et al. (166) created an organic 3.2 V redox-flow battery based upon small molecules. Similar voltage windows can reasonably be expected for polymeric solid-state batteries. Likewise, the capacity of NC-RAPs requires improvement, but many NC-RAPs with high capacities have poor cycling stabilities or low redox potentials. This, too, presents another design opportunity.

Looking to the future, the first translatable applications of organic batteries containing NC-RAPs may be in niche areas where Li-ion batteries have been challenged, such as flexible electronics, bioimplantable electronics, and low-temperature operation. NC-RAPs may not displace Li-ion batteries overnight but instead may find their own use in applications not yet imagined. As further improvements in the chemistry of NC-RAPs are made, they may expand their impact from niche consumer products all the way into larger-scale applications. Therefore, it is important to recognize the future impact of this growing field.

DISCLOSURE STATEMENT

The authors are not aware of any affiliations, memberships, funding, or financial holdings that might be perceived as affecting the objectivity of this review.

ACKNOWLEDGMENTS

This work was supported by grants NSF-DMR-2119672 and NSF-MPS- 2104179 funded by the National Science Foundation. A.D.E. acknowledges support by the National Science Foundation Graduate Research Fellowship under grant DGE:1746932.

LITERATURE CITED

1. Muench S, Wild A, Friebe C, Haupler B, Janoschka T, Schubert US. 2016. Polymer-based organic batteries. *Chem. Rev.* 116:9438–84
2. Wang S, Easley AD, Lutkenhaus JL. 2020. 100th Anniversary of Macromolecular Science Viewpoint: fundamentals for the future of macromolecular nitroxide radicals. *ACS Macro Lett.* 9:358–70
3. Poizot P, Gaubicher J, Renault S, Dubois L, Liang Y, Yao Y. 2020. Opportunities and challenges for organic electrodes in electrochemical energy storage. *Chem. Rev.* 120:6490–557
4. Goujon N, Casado N, Patil N, Marcilla R, Mecerreyes D. 2021. Organic batteries based on just redox polymers. *Prog. Polym. Sci.* 122:101449
5. Esser B. 2019. Redox polymers as electrode-active materials for batteries. *Org. Mater.* 1:63–70
6. Rohland P, Schröter E, Nolte O, Newkome GR, Hager MD, Schubert US. 2022. Redox-active polymers: the magic key towards energy storage—a polymer design guideline progress in polymer science. *Prog. Polym. Sci.* 125:101474
7. Ruff I, Friedrich VJ. 1971. Transfer diffusion. I. Theoretical. *J. Phys. Chem.* 75:3297–302
8. Dahms H. 1968. Electronic conduction in aqueous solution. *J. Phys. Chem.* 72:362–64
9. Sato K, Ichinoi R, Mizukami R, Serikawa T, Sasaki Y, et al. 2018. Diffusion-cooperative model for charge transport by redox-active nonconjugated polymers. *J. Am. Chem. Soc.* 140:1049–56
10. Laviron E. 1980. A multilayer model for the study of space distributed redox modified electrodes: part I. Description and discussion of the model. *J. Electroanal. Chem. Interfacial Electrochem.* 112:1–9
11. Andrieux CP, Savéant JM. 1980. Electron transfer through redox polymer films. *J. Electroanal. Chem. Interfacial Electrochem.* 111:377–81
12. Marcus RA. 1956. On the theory of oxidation-reduction reactions involving electron transfer. I. *J. Chem. Phys.* 24:966–78
13. Marcus RA. 1993. Electron transfer reactions in chemistry. Theory and experiment. *Rev. Mod. Phys.* 65:599–610
14. Marcus RA. 1968. Electron transfer at electrodes and in solution: comparison of theory and experiment. *Electrochim. Acta* 13:995–1004
15. Hush NS. 1958. Adiabatic rate processes at electrodes. I. Energy-charge relationships. *J. Chem. Phys.* 28:962–72
16. Hush NS. 1968. Homogeneous and heterogeneous optical and thermal electron transfer. *Electrochim. Acta* 13:1005–23
17. Ohsaka T, Yamamoto H, Oyama N. 1987. Thermodynamic parameters for charge-transfer reactions in pendant viologen polymers coated on graphite electrodes and at electrode/pendant viologen polymer film interfaces. *J. Phys. Chem.* 91:3775–79
18. von Smoluchowski M. 1906. Zur kinetischen Theorie der Brownschen Molekularbewegung und der Suspensionen. *Ann. Phys* 326:756–80
19. Yoshida N. 1985. Calculation of the self-diffusion coefficient of interacting Brownian particles based on the time-independent Smoluchowski equation. *J. Chem. Phys.* 83:4786–90
20. Akhoury A, Bromberg L, Hatton TA. 2013. Interplay of electron hopping and bounded diffusion during charge transport in redox polymer electrodes. *J. Phys. Chem. B* 117:333–42
21. Kuki A, Wolynes PG. 1987. Electron tunneling paths in proteins. *Science* 236:1647–52

22. Anson FC. 1964. Application of potentiostatic current integration to the study of the adsorption of cobalt(III)-(ethylenedinitrilo)tetraacetate on mercury electrodes. *Anal. Chem.* 36:932–34
23. Anson FC. 1966. Innovations in the study of adsorbed reactants by chronocoulometry. *Anal. Chem.* 38:54–57
24. Zahn R, Coullerez G, Vörös J, Zambelli T. 2012. Effect of polyelectrolyte interdiffusion on electron transport in redox-active polyelectrolyte multilayers. *J. Mater. Chem.* 22:11073–78
25. Wang H, Sayed SY, Luber EJ, Olsen BC, Shirurkar SM, et al. 2020. Redox flow batteries: how to determine electrochemical kinetic parameters. *ACS Nano* 14:2575–84
26. Oyaizu K, Kawamoto T, Suga T, Nishide H. 2010. Synthesis and charge transport properties of redox-active nitroxide polyethers with large site density. *Macromolecules* 43:10382–89
27. Nicholson RS, Shain I. 1964. Theory of stationary electrode polarography. Single scan and cyclic methods applied to reversible, irreversible, and kinetic systems. *Anal. Chem.* 36:706–23
28. Erdey-Grúz T, Volmer M. 2017. Zur theorie der Wasserstoff Überspannung. *Z. Phys. Chem.* 150A(1):203–13
29. Eisner U, Gileadi E. 1970. Anodic oxidation of hydrazine and its derivatives: part 1. The oxidation of hydrazine on gold electrodes in acid solutions. *J. Electroanal. Chem. Interfacial Electrochem.* 28(1):81–92
30. Klingler RJ, Kochi JK. 1981. Electron-transfer kinetics from cyclic voltammetry. Quantitative description of electrochemical reversibility. *J. Phys. Chem.* 85(12):1731–41
31. Bard AJ, Faulkner LR. 2000. *Electrochemical Methods: Fundamentals and Applications*. Hoboken, NJ: John Wiley & Sons. 2nd ed.
32. Ma T, Easley AD, Wang S, Flouda P, Lutkenhaus JL. 2021. Mixed electron-ion-water transfer in macromolecular radicals for metal-free aqueous batteries. *Cell Rep. Phys. Sci.* 2:100414
33. Easley AD, Shaligram SV, Echols IJ, Nixon K, Regen SL, Lutkenhaus JL. 2022. Layer-by-layer nanoarchitectonics of electrochemically active thin films comprised of radical-containing polymers. *J. Electrochem. Soc.* 169:020510
34. Oka K, Kato R, Oyaizu K, Nishide H. 2018. Poly(vinyldibenzothiophenesulfone): its redox capability at very negative potential toward an all-organic rechargeable device with high-energy density. *Adv. Funct. Mater.* 28:1805858
35. Qiu J, Hajibabaei H, Nellist MR, Laskowski FAL, Hamann TW, Boettcher SW. 2017. Direct in situ measurement of charge transfer processes during photoelectrochemical water oxidation on catalyzed hematite. *ACS Cent. Sci.* 3:1015–25
36. Porras-Gutiérrez AG, Frontana-Uribe BA, Gutiérrez-Granados S, Griveau S, Bedioui F. 2013. In situ characterization by cyclic voltammetry and conductance of composites based on polypyrrole, multi-walled carbon nanotubes and cobalt phthalocyanine. *Electrochim. Acta* 89:840–47
37. Salinas G, Frontana-Uribe BA. 2019. Analysis of conjugated polymers conductivity by in situ electrochemical-conductance method. *ChemElectroChem* 6:4105–17
38. Thakur RM, Easley AD, Wang S, Zhang Y, Ober CK, Lutkenhaus JL. 2022. Real time quantification of mixed ion and electron transfer associated with the doping of poly(3-hexylthiophene). *J. Mater. Chem. C* 10:7251–62
39. Rostro L, Wong SH, Boudouris BW. 2014. Solid state electrical conductivity of radical polymers as a function of pendant group oxidation state. *Macromolecules* 47:3713–19
40. Zhang Y, Park A, Cintora A, McMillan SR, Harmon NJ, et al. 2018. Impact of the synthesis method on the solid-state charge transport of radical polymers. *J. Mater. Chem. C* 6:111–18
41. Deng W, Shi W, Liu Q, Jiang J, Wang Q, Guo C. 2020. Conductive nonconjugated radical polymer as high capacity organic cathode material for high-energy Li/Na ion batteries. *J. Power Sources* 479:228796
42. Yu I, Jeon D, Boudouris B, Joo Y. 2020. Mixed ionic and electronic conduction in radical polymers. *Macromolecules* 53:4435–41
43. Joo Y, Agarkar V, Sung SH, Savoie BM, Boudouris BW. 2018. A nonconjugated radical polymer glass with high electrical conductivity. *Science* 359:1391–95
44. Tanaka M, Hatta K, Edura T, Tsutsui K, Wada Y, Nishide H. 2007. Conductive characteristics of radical-bearing polythiophenes using a microcomb-shaped electrode. *Polym. Adv. Technol.* 18:925–31
45. Zhang Y, Park AM, McMillan SR, Harmon NJ, Flatté ME, et al. 2018. Charge transport in conjugated polymers with pendent stable radical groups. *Chem. Mater.* 30:4799–807

46. Wang S, Easley AD, Thakur RM, Ma T, Yun J, et al. 2020. Quantifying internal charge transfer and mixed ion-electron transfer in conjugated radical polymers. *Chem. Sci.* 11:9962–70
47. Häringer D, Novák P, Haas O, Piro B, Pham M-C. 1999. Poly(5-amino-1,4-naphthoquinone), a novel lithium-inserting electroactive polymer with high specific charge. *J. Electrochem. Soc.* 146:2393–96
48. Shen YF, Yuan DD, Ai XP, Yang HX, Zhou M. 2015. High capacity and cycling stability of poly(diaminoanthraquinone) as an organic cathode for rechargeable lithium batteries. *J. Polym. Sci. B* 53:235–38
49. Zhao L, Wang W, Wang A, Yuan K, Chen S, Yang Y. 2013. A novel polyquinone cathode material for rechargeable lithium batteries. *J. Power Sources* 233:23–27
50. Song Z, Zhan H, Zhou Y. 2009. Anthraquinone based polymer as high performance cathode material for rechargeable lithium batteries. *Chem. Commun.* 2009:448–50
51. Deng W, Liang X, Wu X, Qian J, Cao Y, et al. 2013. A low cost, all-organic Na-ion battery based on polymeric cathode and anode. *Sci. Rep.* 3:2671
52. Song Z, Qian Y, Zhang T, Otani M, Zhou H. 2015. Poly(benzoquinonyl sulfide) as a high-energy organic cathode for rechargeable Li and Na batteries. *Adv. Sci.* 2:1500124
53. Tang M, Zhu S, Liu Z, Jiang C, Wu Y, et al. 2018. Tailoring π-conjugated systems: from π-π stacking to high-rate-performance organic cathodes. *Chemistry* 4:2600–14
54. Tang M, Wu Y, Chen Y, Jiang C, Zhu S, et al. 2019. An organic cathode with high capacities for fast-charge potassium-ion batteries. *J. Mater. Chem. A* 7:486–92
55. Petronico A, Bassett KL, Nicolau BG, Gewirth AA, Nuzzo RG. 2017. Toward a four-electron redox quinone polymer for high capacity lithium ion storage. *Adv. Energy Mater.* 8:1700960
56. Kassam A, Burnell DJ, Dahn JR. 2011. Lithiated 1,4,5,8-naphthalenetetraol formaldehyde polymer, an organic cathode material. *Electrochem. Solid-State Lett.* 14:A22
57. Song Z, Qian Y, Liu X, Zhang T, Zhu Y, et al. 2014. A quinone-based oligomeric lithium salt for superior Li–organic batteries. *Energy Environ. Sci.* 7:4077–86
58. Haupler B, Hagemann T, Friebe C, Wild A, Schubert US. 2015. Dithiophenedione-containing polymers for battery application. *ACS Appl. Mater. Interfaces* 7:3473–79
59. Jing Y, Liang Y, Gheytani S, Yao Y. 2017. Cross-conjugated oligomeric quinones for high performance organic batteries. *Nano Energy* 37:46–52
60. Xie J, Wang Z, Xu ZJ, Zhang Q. 2018. Toward a high-performance all-plastic full battery with a single organic polymer as both cathode and anode. *Adv. Energy Mater.* 8:1703509
61. Liu T, Kim KC, Lee B, Chen Z, Noda S, et al. 2017. Self-polymerized dopamine as an organic cathode for Li- and Na-ion batteries. *Energy Environ. Sci.* 10:205–15
62. Pirnat K, Casado N, Porcarelli L, Ballard N, Mecerreyes D. 2019. Synthesis of redox polymer nanoparticles based on poly(vinyl catechols) and their electroactivity. *Macromolecules* 52:8155–66
63. Muench S, Winsberg J, Friebe C, Wild A, Brendel JC, et al. 2018. pNTQS: easily accessible high-capacity redox-active polymer for organic battery electrodes. *ACS Appl. Energy Mater.* 1:3554–59
64. Huang W, Jia T, Zhou G, Chen S, Hou Q, et al. 2018. A triphenylamine-based polymer with anthraquinone side chain as cathode material in lithium ion batteries. *Electrochim. Acta* 283:1284–90
65. Choi W, Harada D, Oyaizu K, Nishide H. 2011. Aqueous electrochemistry of poly(vinylanthraquinone) for anode-active materials in high-density and rechargeable polymer/air batteries. *J. Am. Chem. Soc.* 133:19839–43
66. Kawai T, Oyaizu K, Nishide H. 2015. High-density and robust charge storage with poly(anthraquinone-substituted norbornene) for organic electrode-active materials in polymer–air secondary batteries. *Macromolecules* 48:2429–34
67. Oyaizu K, Choi W, Nishide H. 2011. Functionalization of poly(4-chloromethylstyrene) with anthraquinone pendants for organic anode-active materials. *Polym. Adv. Technol.* 22:1242–47
68. Wang S, Wang Q, Shao P, Han Y, Gao X, et al. 2017. Exfoliation of covalent organic frameworks into few-layer redox-active nanosheets as cathode materials for lithium-ion batteries. *J. Am. Chem. Soc.* 139:4258–61
69. Gu S, Wu S, Cao L, Li M, Qin N, et al. 2019. Tunable redox chemistry and stability of radical intermediates in 2D covalent organic frameworks for high performance sodium ion batteries. *J. Am. Chem. Soc.* 141:9623–28

70. Kang H, Liu H, Li C, Sun L, Zhang C, et al. 2018. Polyanthraquinone-triazine-A promising anode material for high-energy lithium-ion batteries. *ACS Appl. Mater. Interfaces* 10:37023–30
71. Torres W, Fox MA. 1990. Poly(*N*-3-thenylphthalimide): conductivity and spectral properties. *Chem. Mater.* 2:158–62
72. Song Z, Zhan H, Zhou Y. 2010. Polyimides: promising energy-storage materials. *Angew. Chem. Int. Ed.* 49:8444–48
73. Oyaizu K, Hatemata A, Choi W, Nishide H. 2010. Redox-active polyimide/carbon nanocomposite electrodes for reversible charge storage at negative potentials: expanding the functional horizon of polyimides. *J. Mater. Chem.* 20:5404–10
74. Xu F, Xia J, Shi W. 2015. Anthraquinone-based polyimide cathodes for sodium secondary batteries. *Electrochem. Commun.* 60:117–20
75. Wang H-g, Yuan S, Ma D-l, Huang X-l, Meng F-l, Zhang X-b. 2014. Tailored aromatic carbonyl derivative polyimides for high-power and long-cycle sodium-organic batteries. *Adv. Energy Mater.* 4:1301651
76. Xu F, Wang H, Wu M, Nan J, Li T, Cao S-a. 2018. Electrochemical properties of poly(anthraquinonyl imide)s as high-capacity organic cathode materials for Li-ion batteries. *Mater. Chem. Phys.* 214:120–25
77. Chen C, Zhao X, Li H-B, Gan F, Zhang J, et al. 2017. Naphthalene-based polyimide derivatives as organic electrode materials for lithium-ion batteries. *Electrochim. Acta* 229:387–95
78. Sharma P, Damien D, Nagarajan K, Shaijumon MM, Hariharan M. 2013. Perylene-polyimide-based organic electrode materials for rechargeable lithium batteries. *J. Phys. Chem. Lett.* 4:3192–97
79. Liang Y, Chen Z, Jing Y, Rong Y, Facchetti A, Yao Y. 2015. Heavily n-dopable π-conjugated redox polymers with ultrafast energy storage capability. *J. Am. Chem. Soc.* 137:4956–59
80. Li J, Jing X, Li Q, Li S, Gao X, et al. 2020. Bulk COFs and COF nanosheets for electrochemical energy storage and conversion. *Chem. Soc. Rev.* 49:3565–604
81. Wang G, Chandrasekhar N, Biswal BP, Becker D, Paasch S, et al. 2019. A crystalline, 2D polyarylimide cathode for ultrastable and ultrafast Li storage. *Adv. Mater.* 31:e1901478
82. Lv J, Tan YX, Xie J, Yang R, Yu M, et al. 2018. Direct solar-to-electrochemical energy storage in a functionalized covalent organic framework. *Angew. Chem. Int. Ed.* 57:12716–20
83. Tian D, Zhang H-Z, Zhang D-S, Chang Z, Han J, et al. 2014. Li-ion storage and gas adsorption properties of porous polyimides (PIs). *RSC Adv.* 4:7506–10
84. Schon TB, Tilley AJ, Kynaston EL, Seferos DS. 2017. Three-dimensional arylene diimide frameworks for highly stable lithium ion batteries. *ACS Appl. Mater. Interfaces* 9:15631–37
85. Geng J, Bonnet J-P, Renault S, Dolhem F, Poizot P. 2010. Evaluation of polyketones with N-cyclic structure as electrode material for electrochemical energy storage: case of tetraketopiperazine unit. *Energy Environ. Sci.* 3:1929–33
86. Nokami T, Matsuo T, Inatomi Y, Hojo N, Tsukagoshi T, et al. 2012. Polymer-bound pyrene-4,5,9,10-tetraone for fast-charge and -discharge lithium-ion batteries with high capacity. *J. Am. Chem. Soc.* 134:19694–700
87. Liang Y, Jing Y, Gheytani S, Lee KY, Liu P, et al. 2017. Universal quinone electrodes for long cycle life aqueous rechargeable batteries. *Nat. Mater.* 16:841–48
88. Xie J, Chen W, Long G, Gao W, Xu ZJ, et al. 2018. Boosting the performance of organic cathodes through structure tuning. *J. Mater. Chem. A* 6:12985–91
89. Li Q, Li D, Wang H, Wang HG, Li Y, et al. 2019. Conjugated carbonyl polymer-based flexible cathode for superior lithium-organic batteries. *ACS Appl. Mater. Interfaces* 11:28801–8
90. Shi R, Liu L, Lu Y, Li Y, Zheng S, et al. 2020. In situ polymerized conjugated poly(pyrene-4,5,9,10-tetraone)/carbon nanotubes composites for high-performance cathode of sodium batteries. *Adv. Energy Mater.* 11:2002917
91. Trofimov BA, Myachina GF, Rodionova IV, Mal'kina AG, Dorofeev IA, et al. 2008. Ethynedithiol-based polyeneoligosulfides as active cathode materials for lithium-sulfur batteries. *J. Appl. Polymer Sci.* 107:784–87
92. Sarukawa T, Oyama N. 2010. Electrochemical activity of sulfur-linked tetrathionaphthalene polymer. *J. Electrochem. Soc.* 157:F23

93. Su Y-Z, Dong W, Zhang J-H, Song J-H, Zhang Y-H, Gong K-C. 2007. Poly[bis(2-aminophenyloxy)disulfide]: a polyaniline derivative containing disulfide bonds as a cathode material for lithium battery. *Polymer* 48:165–73
94. Simmonds AG, Griebel JJ, Park J, Kim KR, Chung WJ, et al. 2014. Inverse vulcanization of elemental sulfur to prepare polymeric electrode materials for Li–S batteries. *ACS Macro Lett.* 3:229–32
95. Grocke GL, Zhang H, Kopfinger SS, Patel SN, Rowan SJ. 2021. Synthesis and characterization of redox-responsive disulfide cross-linked polymer particles for energy storage applications. *ACS Macro Lett*. 10:1637–42
96. Nakahara K, Iwasa S, Satoh M, Morioka Y, Iriyama J, et al. 2002. Rechargeable batteries with organic radical cathodes. *Chem. Phys. Lett.* 359:351–54
97. Wang S, Li F, Easley AD, Lutkenhaus JL. 2019. Real-time insight into the doping mechanism of redox-active organic radical polymers. *Nat. Mater.* 18:69–75
98. Wang S, Park AMG, Flouda P, Easley AD, Li F, et al. 2020. Solution-processable thermally crosslinked organic radical polymer battery cathodes. *ChemSusChem* 13:2371–78
99. Qin H, Liu X, Huang J, Liang H, Zhang Z, Lu J. 2019. Design and synthesis of a facile solution-processing and ultrastable crosslinkable branched nitroxide polymer. *Macromol. Chem. Phys.* 220:1900068
100. Rohan R, Hung M-K, Yang Y-F, Hsu C-W, Yeh C-K, et al. 2022. Enhancement of the high-rate performance of an organic radical thin-film battery by decreasing the grafting density of polymer brushes. *ACS Appl. Polym. Mater*. 4:2365–72
101. López-Peña HA, Hernández-Muñoz LS, Cardoso J, González FJ, González I, Frontana C. 2009. Electrochemical and spectroelectrochemical properties of nitroxyl radical species in PTMA, an organic radical polymer. Influence of the microstructure. *Electrochem. Commun.* 11:1369–72
102. Guo W, Yin Y-X, Xin S, Guo Y-G, Wan L-J. 2012. Superior radical polymer cathode material with a two-electron process redox reaction promoted by graphene. *Energy Environ. Sci.* 5:5221–25
103. Qu J, Khan FZ, Satoh M, Wada J, Hayashi H, et al. 2008. Synthesis and charge/discharge properties of cellulose derivatives carrying free radicals. *Polymer* 49:1490–96
104. Nesvadba P, Bugnon L, Maire P, Novák P. 2009. Synthesis of a novel spirobisnitroxide polymer and its evaluation in an organic radical battery. *Chem. Mater.* 22:783–88
105. Oyaizu K, Suga T, Yoshimura K, Nishide H. 2008. Synthesis and characterization of radical-bearing polyethers as an electrode-active material for organic secondary batteries. *Macromolecules* 41:6646–52
106. Anghel M, Magnan F, Catingan SD, McCready MA, Aawani E, et al. 2020. Redox polymers incorporating pendant 6-oxoverdazyl and nitronyl nitroxide radicals. *J. Polym. Sci.* 58:309–19
107. Ezugwu S, Paquette JA, Yadav V, Gilroy JB, Fanchini G. 2016. Design criteria for ultrathin single-layer flash memristors from an organic polyradical. *Adv. Electron. Mater.* 2:1600253
108. Hansen KA, Nerkar J, Thomas K, Bottle SE, O'Mullane AP, et al. 2018. New spin on organic radical batteries—an isoindoline nitroxide-based high-voltage cathode material. *ACS Appl. Mater. Interfaces* 10:7982–88
109. Suga T, Sugita S, Ohshiro H, Oyaizu K, Nishide H. 2011. p- and n-type bipolar redox-active radical polymer: toward totally organic polymer-based rechargeable devices with variable configuration. *Adv. Mater.* 23:751–54
110. Xiong J, Wei Z, Xu T, Zhang Y, Xiong C, Dong L. 2017. Polytriphenylamine derivative with enhanced electrochemical performance as the organic cathode material for rechargeable batteries. *Polymer* 130:135–42
111. Jähnert T, Hager MD, Schubert US. 2016. Assorted phenoxyl-radical polymers and their application in lithium-organic batteries. *Macromol. Rapid Commun.* 37:725–30
112. Saal A, Friebe C, Schubert US. 2022. Blatter radical as a polymeric active material in organic batteries. *J. Power Sources* 524:231061
113. Gerlach P, Burges R, Lex-Balducci A, Schubert US, Balducci A. 2019. Influence of the salt concentration on the electrochemical performance of electrodes for polymeric batteries. *Electrochim. Acta* 306:610–16
114. Easley AD, Vukin LM, Flouda P, Howard DL, Pena JL, Lutkenhaus JL. 2020. Nitroxide radical polymer–solvent interactions and solubility parameter determination. *Macromolecules* 53:7997–8008

115. Feng JK, Cao YL, Ai XP, Yang HX. 2008. Polytriphenylamine: a high power and high capacity cathode material for rechargeable lithium batteries. *J. Power Sources* 177:199–204
116. Su C, Yang F, Ji L, Xu L, Zhang C. 2014. Polytriphenylamine derivative with high free radical density as the novel organic cathode for lithium ion batteries. *J. Mater. Chem. A* 2:20083–88
117. Obrezkov FA, Shestakov AF, Traven VF, Stevenson KJ, Troshin PA. 2019. An ultrafast charging polyphenylamine-based cathode material for high rate lithium, sodium and potassium batteries. *J. Mater. Chem. A* 7:11430–37
118. Obrezkov FA, Ramezankhani V, Zhidkov I, Traven VF, Kurmaev EZ, et al. 2019. High-energy and high-power-density potassium ion batteries using dihydrophenazine-based polymer as active cathode material. *J. Phys. Chem. Lett.* 10:5440–45
119. Lee M, Hong J, Lee B, Ku K, Lee S, et al. 2017. Multi-electron redox phenazine for ready-to-charge organic batteries. *Green Chem.* 19:2980–85
120. Kolek M, Otteny F, Becking J, Winter M, Esser B, Bieker P. 2018. Mechanism of charge/discharge of poly(vinylphenothiazine)-based Li–organic batteries. *Chem. Mater.* 30:6307–17
121. Otteny F, Perner V, Einholz C, Desmaizieres G, Schleicher E, et al. 2021. Bridging the gap between small molecular π-interactions and their effect on phenothiazine-based redox polymers in organic batteries. *ACS Appl. Energy Mater.* 4:7622–31
122. Otteny F, Kolek M, Becking J, Winter M, Bieker P, Esser B. 2018. Unlocking full discharge capacities of poly(vinylphenothiazine) as battery cathode material by decreasing polymer mobility through cross-linking. *Adv. Energy Mater.* 8:1802151
123. Schmidt M, Hermann M, Otteny F, Esser B. 2020. Calix[*n*]phenothiazines: optoelectronic and structural properties and host–guest chemistry. *Org. Mater.* 02:235–39
124. Peterson BM, Ren D, Shen L, Wu Y-CM, Ulgut B, et al. 2018. Phenothiazine-based polymer cathode materials with ultrahigh power densities for lithium ion batteries. *ACS Appl. Energy Mater.* 1:3560–64
125. Kuzin YI, Khadieva AI, Padnya PL, Khannanov AA, Kutyreva MP, et al. 2021. Electrochemistry of new derivatives of phenothiazine: electrode kinetics and electropolymerization conditions. *Electrochim. Acta* 375:137985
126. Otteny F, Perner V, Wassy D, Kolek M, Bieker P, et al. 2019. Poly(vinylphenoxazine) as fast-charging cathode material for organic batteries. *ACS Sustain. Chem. Eng.* 8:238–47
127. Speer ME, Kolek M, Jassoy JJ, Heine J, Winter M, et al. 2015. Thianthrene-functionalized polynorbornenes as high-voltage materials for organic cathode-based dual-ion batteries. *Chem. Commun.* 51:15261–64
128. Wild A, Strumpf M, Häupler B, Hager MD, Schubert US. 2017. All-organic battery composed of thianthrene- and TCAQ-based polymers. *Adv. Energy Mater.* 7:1601415
129. Acker P, Speer ME, Wössner JS, Esser B. 2020. Azine-based polymers with a two-electron redox process as cathode materials for organic batteries. *J. Mater. Chem. A* 8:11195–201
130. Li C, Xue J, Huang A, Ma J, Qing F, et al. 2019. Poly(N-vinylcarbazole) as an advanced organic cathode for potassium-ion-based dual-ion battery. *Electrochim. Acta* 297:850–55
131. Yao M, Senoh H, Sakai T, Kiyobayashi T. 2012. Redox active poly(*N*-vinylcarbazole) for use in rechargeable lithium batteries. *J. Power Sources* 202:364–68
132. Sano N, Tomita W, Hara S, Min C-M, Lee J-S, et al. 2013. Polyviologen hydrogel with high-rate capability for anodes toward an aqueous electrolyte-type and organic-based rechargeable device. *ACS Appl. Mater. Interfaces* 5:1355–61
133. Beladi-Mousavi SM, Sadaf S, Mahmood AM, Walder L. 2017. High performance poly(viologen)–graphene nanocomposite battery materials with puff paste architecture. *ACS Nano* 11:8730–40
134. Nguyen TP, Easley AD, Kang N, Khan S, Lim S-M, et al. 2021. Polypeptide organic radical batteries. *Nature* 593:61–66
135. Li F, Gore DN, Wang S, Lutkenhaus JL. 2017. Unusual internal electron transfer in conjugated radical polymers. *Angew. Chem. Int. Ed.* 56:9856–59
136. Wang W, Zhao C, Yang J, Xiong P, Su H, Xu Y. 2021. *In-situ* electropolymerized bipolar organic cathode for stable and high-rate lithium-ion batteries. *Sci. China Mater.* 64:2938–48

137. Zhao Y, Wu M, Chen H, Zhu J, Liu J, et al. 2021. Balance cathode-active and anode-active groups in one conjugated polymer towards high-performance all-organic lithium-ion batteries. *Nano Energy* 86:106055
138. Casado N, Mantione D, Shanmukaraj D, Mecerreyes D. 2020. Symmetric all-organic battery containing a dual redox-active polymer as cathode and anode material. *ChemSusChem* 13:2464–70
139. Li W, Jiang S, Xie Y, Yan X, Zhao F, et al. 2022. Anthraquinone-catalyzed TEMPO reduction to realize two-electron energy storage of poly(TEMPO-methacrylate). *ACS Energy Lett.* 7:1481–89
140. Zhao Y, Wu M, Zhang H, Ge Z, Li C, et al. 2022. One polymer with three charge states for two types of lithium-ion batteries with different characteristics as needed. *Energy Storage Mater.* 47:141–48
141. Zhang K, Xie Y, Noble BB, Monteiro MJ, Lutkenhaus JL, et al. 2021. Unravelling kinetic and mass transport effects on two-electron storage in radical polymer batteries. *J. Mater. Chem. A* 9:13071–79
142. Qu J, Morita R, Satoh M, Wada J, Terakura F, et al. 2008. Synthesis and properties of DNA complexes containing 2,2,6,6-tetramethyl-1-piperidinoxy (TEMPO) moieties as organic radical battery materials. *Chemistry* 14:3250–59
143. Huang Q, Choi D, Cosimbescu L, Lemmon JP. 2013. Multi-electron redox reaction of an organic radical cathode induced by a mesopore carbon network with nitroxide polymers. *Phys. Chem. Chem. Phys.* 15:20921–28
144. Li Y, Jian Z, Lang M, Zhang C, Huang X. 2016. Covalently functionalized graphene by radical polymers for graphene-based high-performance cathode materials. *ACS Appl. Mater. Interfaces* 8:17352–59
145. Zhou T, Jin W, Xue W, Dai B, Feng C, et al. 2021. Radical polymer-grafted carbon nanotubes as high-performance cathode materials for lithium organic batteries with promoted n-/p-type redox reactions. *J. Power Sources* 483:229136
146. Deng Y, Teng C, Wu Y, Zhang K, Yan L. 2022. Polypeptide radical cathode for aqueous Zn-ion battery with two-electron storage and faster charging rate. *ChemSusChem* 15:e202102710
147. Su C, Yang F, Xu L, Zhu X, He H, Zhang C. 2015. Radical polymer containing a polytriphenylamine backbone: its synthesis and electrochemical performance as the cathode of lithium-ion batteries. *ChemPlusChem* 80:606–11
148. Sukegawa T, Kai A, Oyaizu K, Nishide H. 2013. Synthesis of pendant nitronyl nitroxide radical-containing poly(norbornene)s as ambipolar electrode-active materials. *Macromolecules* 46:1361–67
149. Suga T, Pu Y-J, Kasatori S, Nishide H. 2007. Cathode- and anode-active poly(nitroxylstyrene)s for rechargeable batteries: p- and n-type redox switching via substituent effects. *Macromolecules* 40:3167–73
150. Jähnert T, Janoschka T, Hager MD, Schubert US. 2014. Polymers with n-type nitroxide side groups: synthesis and electrochemical characterization. *Eur. Polym. J.* 61:105–12
151. Paquette JA, Ezugwu S, Yadav V, Fanchini G, Gilroy JB. 2016. Synthesis, characterization, and thin-film properties of 6-oxoverdazyl polymers prepared by ring-opening metathesis polymerization. *J. Polym. Sci. A* 54:1803–13
152. Price JT, Paquette JA, Harrison CS, Bauld R, Fanchini G, Gilroy JB. 2014. 6-Oxoverdazyl radical polymers with tunable electrochemical properties. *Polym. Chem.* 5:5223–26
153. Magnan F, Dhindsa JS, Anghel M, Bazylewski P, Fanchini G, Gilroy JB. 2021. A divergent strategy for the synthesis of redox-active verdazyl radical polymers. *Polym. Chem.* 12:2786–97
154. Sentyurin VV, Levitskiy OA, Magdesieva TV. 2020. Molecular design of ambipolar redox-active open-shell molecules: principles and implementations. *Curr. Opin. Electrochem.* 24:15–23
155. Magdesieva T. 2022. Ambipolar diarylnitroxides: molecular design and electrochemical testing. *Electrochem. Sci. Adv.* 2(6):e2100182
156. Li C-H, Tabor DP. 2022. Discovery of lead low-potential radical candidates for organic radical polymer batteries with machine-learning-assisted virtual screening. *J. Mater. Chem. A* 10:8273–82
157. Poizot P, Dolhem F, Gaubicher J. 2018. Progress in all-organic rechargeable batteries using cationic and anionic configurations: Toward low-cost and greener storage solutions? *Curr. Opin. Electrochem.* 9:70–80
158. Zhu LM, Lei AW, Cao YL, Ai XP, Yang HX. 2013. An all-organic rechargeable battery using bipolar polyparaphenylene as a redox-active cathode and anode. *Chem. Commun.* 49:567–69
159. Wang H, Emanuelsson R, Karlsson C, Jannasch P, Strømme M, Sjödin M. 2021. Rocking-chair proton batteries with conducting redox polymer active materials and protic ionic liquid electrolytes. *ACS Appl. Mater. Interfaces* 13:19099–108

160. Yao M, Sano H, Ando H, Kiyobayashi T. 2015. Molecular ion battery: a rechargeable system without using any elemental ions as a charge carrier. *Sci. Rep.* 5:10962
161. Chikushi N, Yamada H, Oyaizu K, Nishide H. 2012. TEMPO-substituted polyacrylamide for an aqueous electrolyte-typed and organic-based rechargeable device. *Sci. China Chem.* 55:822–29
162. Wang H, Wu Q, Wang Y, Lv X, Wang H-g. 2022. A redox-active metal–organic compound for lithium/sodium-based dual-ion batteries. *J. Colloid Interface Sci.* 606:1024–30
163. Zhang Y, An Y, Yin B, Jiang J, Dong S, et al. 2019. A novel aqueous ammonium dual-ion battery based on organic polymers. *J. Mater. Chem. A* 7:11314–20
164. Suga T, Ohshiro H, Sugita S, Oyaizu K, Nishide H. 2009. Emerging N-type redox-active radical polymer for a totally organic polymer-based rechargeable battery. *Adv. Mater.* 21:1627–30
165. Tan Y, Casetti NC, Boudouris BW, Savoie BM. 2021. Molecular design features for charge transport in nonconjugated radical polymers. *J. Am. Chem. Soc.* 143:11994–2002
166. Yan Y, Robinson SG, Sigman MS, Sanford MS. 2019. Mechanism-based design of a high-potential catholyte enables a 3.2 V all-organic nonaqueous redox flow battery. *J. Am. Chem. Soc.* 141:15301–6

Annual Review of Chemical and Biomolecular Engineering

Volume 14, 2023

Contents

Errata

An online log of corrections to *Annual Review of Chemical and Biomolecular Engineering* articles may be found at http://www.annualreviews.org/errata/chembioeng